ESA CONTRACT REPORT

European Space Agency Contract Report

Extension of the OSSE Data Base to Scatterometer and ATOVS Data

Authors: Hervé Roquet, Bernd Becker and Roger Saunders*

ESA Contract No: 10921/94/NL/CN

ESA Study Manager: M Wintzer

* *Current affiliation: Météo-France, Toulouse, France*

European Centre for Medium-Range Weather Forecasts
Europäisches Zentrum für mittelfristige Wettervorhersage
Centre européen pour les prévisions météorologiques à moyen terme

European Space Agency Contract Report

Extension of the OSSE Data Base to Scatterometer and ATOVS Data

Hervé Roquet, Bernd Becker and Roger Saunders*

European Centre for Medium-Range Weather Forecasts
Shinfield Park, Reading, Berkshire, UK

ESA Contract No: 10921/94/NL/CN

ESA Study Manager: M Wintzer

* *Current affiliation: Météo-France, Toulouse, France*

October 1995

EXECUTIVE SUMMARY

For the purposes of Numerical Weather Prediction (NWP), the coverage of the current network of conventional observations suffers from many gaps, especially over the oceans. This is the reason why, in the last two decades, considerable effort has been put into complementary space-based remote sensing systems. However, there are difficulties which arise when using them in NWP: some of them have a low vertical resolution and an indirect link with atmospheric state variables (e.g. TIROS-N Operational Vertical Sounder (TOVS) data), some others are single level data (e.g. ERS-1 scatterometer data). Doppler Wind Lidar (DWL) data seem very promising because wind is the most important parameter in the tropics at synoptic scales, and everywhere at smaller horizontal scales. However, the contribution of DWL data to NWP will depend not only on their amount, quality and distribution, but also on the other observing systems, which will exist at the time when a space-borne DWL could be flown. A data base of simulated observations dedicated to Observing System Simulation Experiments (OSSE), including DWL measurements, was produced at ECMWF in a previous ESA-funded project. The aim of the present project is to complete this data base with two new satellite instruments, the Advanced SCATterometer (ASCAT) and the Advanced TIROS-N Operational Vertical Sounder (ATOVS), which will be available from meteorological operational satellites in the near future.

ASCAT is a side-looking radar instrument, which will be flown by the future European meteorological polar orbiting satellites. Over sea, this instrument can provide the 10-metre wind vector with a good precision, on two 500 km wide swaths. The ASCAT backscatter measurements are simulated with a 50 km horizontal sampling, for a single polar orbiting satellite. ATOVS is the new atmospheric sounding system of the next NOAA satellites, and differs from the current TOVS by the Advanced Microwave Sounding Units (AMSU-A and B) replacing the current Microwave Sounding Unit (MSU) and Stratospheric Sounding Unit (SSU). ATOVS measurements are simulated as clear-column brightness temperatures, corrected for surface emissivity effects. Their coverage imitates the current NOAA two-satellite system, with the characteristics of the 120 km products generated and distributed operationally by NOAA/NESDIS.

The nature run, i.e. the 30-day numerical weather forecast used to generate the atmospheric fields, is performed with ECMWF's Integrated Forecast System (IFS) model, with a T213 spectral truncation (equivalent horizontal resolution ≈ 80 km) and 31 levels in the vertical. To ensure consistency with the data base produced in the first project, the IFS model is used in an identical version, with identical initial conditions taken from the operational analysis on 5 February 1993 at 00 UT.

In the nature run, ASCAT observations are simulated as 10 metre wind vectors, interpolated from the lowest IFS model level (≈ 32 m) to the locations provided by the orbit simulator. ATOVS brightness temperatures are computed directly in the IFS model by the fast radiative transfer model RTTOV, used primarily for TOVS channels and adapted for the new ATOVS microwave channels. The input temperature and humidity profiles, needed by RTTOV at fixed pressure levels, are interpolated/extrapolated from the nature run temperature and humidity fields.

A post-processor is then used to compute the ASCAT backscatter measurements to add errors to all simulated "true" observations, and to encode them into Binary Universal Format Record (BUFR) format (~ 14 Mbytes per day). For ASCAT data, errors are generated in a two-step procedure, adding first a 1.6 m/s gaussian error to the "true" 10-metre wind components, and then a gaussian error to the backscatter measurements (σ_0's), with a signal-to-noise ratio depending on the wind speed. σ_0's are computed using the CMOD4 transfer function, which was derived for ERS-1 backscatter measurements from ECMWF analysed 10-metre winds. For each ATOVS channel, gaussian errors

or gross errors are alternatively generated independently according to predefined statistics. These statistics are dependent on the chosen cloud-clearing route for the infra-red channels.

To store the simulated observations existing standard BUFR formats are used. The BUFR format of ASCAT data is identical to the current one of ERS-1 scatterometer data, and the BUFR format of TOVS data has been extended to handle the forty ATOVS channels. Inside each BUFR report, extra information is stored in appendices, such as nature run values, and statistical parameters used to generate the random errors.

Each element of the production chain was checked separately. Moreover, the final BUFR products of the data base were validated extensively. The noisy ASCAT backscatter measurements were inverted, and the retrieved winds were compared with the input winds. The noisy TOVS brightness temperatures were inverted by ECMWF's PRESAT procedure, and the retrieved temperature and humidity profiles were checked against the corresponding nature run profiles, used by PRESAT as background, also validating the ATOVS infra-red channels indirectly. Finally, a short assimilation experiment was run within the ECMWF assimilation system at spectral resolution T106 (equivalent horizontal resolution $\approx$ 150 km), using all conventional and TOVS simulated observations.

CONTENTS

1. INTRODUCTION

The accuracy of a forecast from a Numerical Weather Prediction (NWP) system depends not only on a realistic computer model of the atmosphere, but also on a very accurate description of the initial state of the atmosphere, from which the subsequent forecast evolves. The accuracy of the analysis of the initial state is highly dependent on the observation coverage, spatial and temporal resolution, and accuracy. Over oceans, which cover most of the earth's surface, the coverage of "conventional" observations (i.e. from surface stations/platforms, from balloons and from aircraft) is very sparse. Space-based systems offer the only realistic hope of meeting the requirements of operational meteorology for a global coverage of observations with adequate spatial and temporal resolution. The main variables that must be observed in order to specify the initial state of the atmosphere are the three-dimensional fields of temperature, humidity and wind. For an adequate description of the atmosphere on scales represented by most of the present global NWP models, observations are needed at a 50-100 km resolution in the horizontal, ~ 1 km in the vertical, from the surface to about 30 km altitude. In the mid and high latitudes, the temperature and wind fields are coupled through the dynamical equations governing the atmospheric motion. However, there is a significant component of the flow on small horizontal scales which is not coupled, making measurements of wind useful and important, even in the presence of temperature observations. In the tropics the coupling is much weaker and the wind field cannot be inferred, even approximately, from the temperature field. Thus direct observations of wind are even more important here.

At present neither the temperature/humidity nor the wind field is adequately observed from space. An operational systen called TOVS (TIROS-N Operational Vertical Sounder) on the NOAA satellite series provides information on temperature and humidity with adequate temporal and horizontal resolution but poor vertical resolution. The next generation of instruments, the Advanced TOVS (ATOVS) scheduled for first launch in 1996, will provide improved performance in cloudy areas, but will not improve significantly on vertical resolution in the troposphere. Towards the beginning of the next decade infra-red instruments of high spectral resolution, such as Europe's Infra-red Atmospheric Sounding Interferometer (IASI), will offer significant improvement in vertical resolution, approaching the requirements for temperature and humidity information, at least in cloud-free areas. The prospects for improved global, three-dimensional wind observation in the short/medium term are not as good. Scatterometers, such as available from ERS-1 and 2 and expected from other future platforms, give information on the wind field only at the sea surface. The instrument which offers the best long-term prospect of filling this gap is the Doppler Wind Lidar (DWL). However the technology for a space-based system is not well-advanced, and its development will be relatively expensive. It is therefore

important that the capabilities of proposed DWL systems are properly analysed, both as independent systems and also from the perspective of their contribution to the combined global observing system. In particular, their potential impact on NWP can be assessed by Observing System Simulation Experiments (OSSEs), based on realistically simulated observations from the existing and future systems.

At present, ECMWF has completed a first ESA study contract, "Theoretical studies of the impact of Doppler Wind Lidar (DWL) data. Preparation of a data base". This covers the simulation of the following data sets with realistic coverage and error characteristics:

- Conventional observations (SYNOP, SHIP, DRIBU, TEMP, PILOT) + AIREPs + SATOB cloud-tracked winds,
- TOVS clear-column brightness temperatures,
- DWL line-of-sight wind profiles.

The main purpose of this data base is to allow the potential DWL impact on NWP to be assessed. However, a rigorous assessment of DWL impact should take into account the availability of other systems expected to be operational at the time when DWL could be flown (i.e. the next century). Consequently, we have simulated observations from the following new satellite systems, which will be available at that time:

- Advanced SCATterometer (ASCAT), a double swath scatterometer which will be very similar to the single swath ones flown by ERS-1 and 2, and will be part of the payload of the European meteorological polar satellites (METOP).
- Advanced TOVS (ATOVS), which will replace TOVS on the NOAA operational polar-orbiters from 1996, and is planned to continue as the operational sounder on the American and European polar systems which follow the NOAA series.

The observations from these new systems have been simulated fully consistently with the ones of the first project. They have been produced on the same 30-day period, using the same version of the Integrated Forecasting System (IFS), and starting from the same operational ECMWF analysis. The contents of the data base and the 30-day run of the IFS model are reviewed in section 2 and 3 respectively. In section 4 we describe the specific pre-processor, observation simulator and post-processor which have been developed for ASCAT and ATOVS observations. The pre-processor generates the observation location in space and time, which is used subsequently by IFS to compute

the "true" observation values. The post-processor computes the final "noisy" observation values, which are converted into the Binary Universal Format Representation (BUFR). The output BUFR files also contain all the "true" observation values, and the statistical data which have been used to generate the observation errors, which makes the data base very flexible. Section 5 describes the tests which were performed to validate each element of the production chain, and the final data base. A summary and some concluding remarks are given in section 6.

2. CONTENTS OF THE DATA BASE

2.1 ASCAT

The scatterometer is a side-looking radar instrument, measuring the power backscattered towards the satellite by the earth's surface. ASCAT is very similar to the ERS-1 and 2 scatterometers, operating in C-band (5.3 GHz), but with a 500 km wide swath on each side of the satellite. It has three antennae on each side, pointing in a horizontal plane towards a direction of 45°, 90° and 135° with respect to the sub-satellite track. For each antenna, the return signal is sampled every 25 km in both along and across-track directions, to compute a mean backscatter measurement (hereafter denoted σ_0). Over sea, this instrumental quantity can be, with a good precision, related to the 10 metre wind vector (*Stoffelen and Anderson*, 1993), using an empirical transfer function. In the present data base, σ_0 was simulated using the 10-metre wind vector from the IFS model, and the CMOD4 transfer function (*Stoffelen and Anderson*, 1993), which has been determined and calibrated from ERS-1 backscatter measurements and ECMWF 10-metre analysed winds. The details about CMOD4, and the error generation procedure are given in section 4.3.1.

The ASCAT measurements have been simulated with a horizontal sampling distance of 50 km, to be compatible with the horizontal scales which the IFS model can resolve at spectral truncation T213 (equivalent horizontal resolution ≈ 80 km). The METOP orbital parameters, used to generate the location of the ASCAT measurements, are:

Orbit height:	829 km
Orbit inclination:	98.70°
Local equator crossing time (ascending):	0600 UT

We used the following specifications for the ASCAT geometry: a double swath of 500 km width, and an incidence angle at the surface of the earth of 25° for the mid beam at the edge of the first cell. Table 2.1 gives the correspondence between cell number, distance from satellite track, satellite incidence angle (i.e. with respect to the satellite's nadir) and mid beam local incidence angle (i.e. with respect to the vertical on earth's surface) at the centre of each cell, for a 50 km horizontal sampling.

Table 2.1: Characteristics of ASCAT geometry on earth's surface.

Cell number	Distance from satellite track (km)	Satellite incidence angle (deg)	Local incidence angle (mid beam)
1	350	22.67	25.83
3	400	25.44	29.04
5	450	28.05	32.10
7	500	30.51	35.01
9	550	32.81	37.76
11	600	34.97	40.37
13	650	36.99	42.84
15	700	38.87	45.17
17	750	40.62	47.37
19	800	42.24	49.44
21	850	43.76	51.40

2.2 ATOVS

The new sounding system of the next NOAA satellites, called ATOVS, consists of three components: the High-resolution Infra-red Radiation Sounder (HIRS), and the Advanced Microwave Sounding Units (AMSU-A and B). The difference from the current TOVS system is that AMSU-A and B replace the current Microwave Sounding Unit (MSU) and Stratospheric Sounding Unit (SSU). AMSU-A has 15 channels, which are mainly designed for vertical temperature soundings in the troposphere and the stratosphere, but which can also be used to derive integrated water vapour and cloud liquid water contents, and some surface informations (e.g. sea ice, snow...). AMSU-B has 5 channels, designed for vertical tropospheric humidity soundings and higher resolution surface information. This improvement on the microwave part of the current TOVS system (MSU has only 4 channels) is of importance for global coverage, as microwave channels can provide information even in cloudy areas. The main characteristics of these channels are listed in Table 2.2, partly from *Saunders* (1994).

Table 2.2: Characteristics of AMSU-A and B microwave channels.

Channel number	Central frequencies GHZ	Assumed radiometric noise in K	Peak energy level and/or parameter
1	23.8	0.30	Total column water vapour
2	31.4	0.37	Surface parameters
3	50.3	0.37	Surface parameters
4	52.8	0.25	1000 hPa temperature
5	53.596 ± 0.115	0.27	700 hPa temperature
6	54.4	0.25	400 hPa temperature
7	54.94	0.25	250 hPa temperature
8	55.5	0.28	150 hPa temperature
9	ν_1*	0.28	90 hPa temperature
10	$\nu_1 \pm 0.217$*	0.40	50 hPa temperature
11	$\nu_1 \pm \nu_2 \pm 0.048$*	0.42	25 hPa temperature
12	$\nu_1 \pm \nu_2 \pm 0.022$*	0.63	10 hPa temperature
13	$\nu_1 \pm \nu_2 \pm 0.010$*	0.88	5 hPa temperature
14	$\nu_1 \pm \nu_2 \pm 0.0045$*	1.44	2.5 hPa temperature
15	89.0	0.11	Surface parameters
16	89.0	0.11	Surface parameters
17	150.0	0.11	Surface parameters / lower tropospheric humidity
18	183.31 ± 1.0	0.33	Upper tropospheric humidity
19	183.31 ± 3.0	0.33	Mid tropospheric humidity
20	183.31 ± 7.0	0.33	Lower tropospheric humidity

* $\nu_1 = 57.290344$, $\nu_2 = 0.3222$

We have simulated the ATOVS clear-column brightness temperatures in a very similar way to the TOVS in the previous project. The same orbit simulator has been used to reproduce a two-satellite system, similar to the present operational configuration of the NOAA satellites, and the density and coverage imitate the characteristics of the current "120 km BUFR TOVS" data set, generated and distributed operationally by NOAA/NESDIS. The ATOVS brightness temperatures have been generated within the IFS model, using a surface emissivity of one for all channels, as for the TOVS brightness temperatures in the first project. So, the simulated ATOVS brightness temperatures represent pre-processed brightness temperatures, which have been corrected for surface emissivity effects, as is the current case for the NESDIS product, received operationally at ECMWF. This choice was made to allow users to apply their own emissivity correction if required particularly for the microwave channels. The cloud-clearing route decision algorithm for infra-red channels, and the error generation are described in section 4.3.2.

3. NATURE RUN

The nature run is the 30-day integration of the IFS model, providing the state of the atmosphere from which the observations in the data base are simulated. The chosen period is from 5 February to 6 March 1993. The IFS was run in its T213L31 version (equivalent horizontal resolution ≈ 80 km, 31 vertical levels). The vertical levels of the model are listed in Table 3.1.

Table 3.1: Reference pressure levels and reference height levels for the 31 level IFS forecast model.

Level number	P (hPa) L31	Z (km) L31
1	10	31.0
2	30	24.5
3	50	20.5
4	70	18.2
5	90	17.0
6	111	15.5
7	132	14.2
8	156	13.2
9	181	12.5
10	209	11.5
11	238	10.5
12	270	9.7
13	304	9.0
14	340	8.2
15	378	7.5
16	417	6.7
17	458	6.0
18	500	5.2
19	543	4.7
20	588	4.2
21	633	3.7
22	680	3.2
23	726	2.7
24	772	2.2
25	818	1.7
26	861	1.3
27	903	1.0
28	940	0.7
29	972	0.4
30	996	0.15
31	1009	0.03

At each of these levels, the IFS model provides temperature, humidity, wind, cloud cover and cloud liquid vapour content. For the extension of the data base, the most important thing was to ensure and to check the consistency of the new nature run with the one which was used for the generation of the initial data base. We used exactly the same version of the IFS model, which was re-started every day

from the restart files of the first nature run. Moreover, the output fields from the second nature run were saved for different dates, and checked against the ones of the first nature run.

A brief description of the prevailing meteorological situation during this period is given in the contract report of the first project (*Stoffelen et al*, 1994).

4. GENERATION OF THE DATA BASE

The Integrated Forecasting System (IFS) has been developed in co-operation between ECMWF and Météo-France. It involves not only a numerical atmospheric model, but also a lot of modules necessary for the numerous tasks associated with NWP. Among these, the IFS allows a meteorological forecast (the nature run) to run, and comparison of its results with a set of observations at predefined locations at the same time.

For the generation of the data base, the strategy is very similar to the one of the first project. An orbit simulator is used to provide the pre-processor with the space and time locations of the observations. For each 24-hour period starting at 00 UT, the pre-processor splits them into 24 hourly files centred around each full hour, in the so-called Central Memory Arrays (CMA) format. The IFS reads in the 24 files and completes them with the model value at the requested location for the requested variable. The post-processor computes the final observed quantity from the model variable if necessary, adds to it a random error consistently with a predefined error model and converts the internal ECMWF CMA format to standard Binary Universal Format Representation (BUFR) format.

4.1 **Pre-processor**

4.1.1 *ASCAT*

An orbit simulator has been developed for ASCAT measurements, following the specifications given in section 2.1. As the scatterometer provides information on surface wind over open sea only, land and sea ice points had to be eliminated. In order to decrease the number of observation locations, and hence the Central Memory requirements for the observation simulator, this screening was performed within the orbit simulator, using the operational ECMWF land/sea mask and Sea Surface Temperature (SST) analysis. We used the SST analysis on 5 February 1993 for the whole 30-day period, consistently with the nature run. An example of ASCAT coverage for 12 hours is given in Figure 4.1, as produced by the ASCAT orbit simulator.

After the orbit simulator, ASCAT space and time locations are converted to the CMA format. This format has been adapted to handle time information at the accuracy of one second and to store additional parameters needed further as an input for σ_0's computation (node number, mid beam incidence angle, mid beam azimuth).

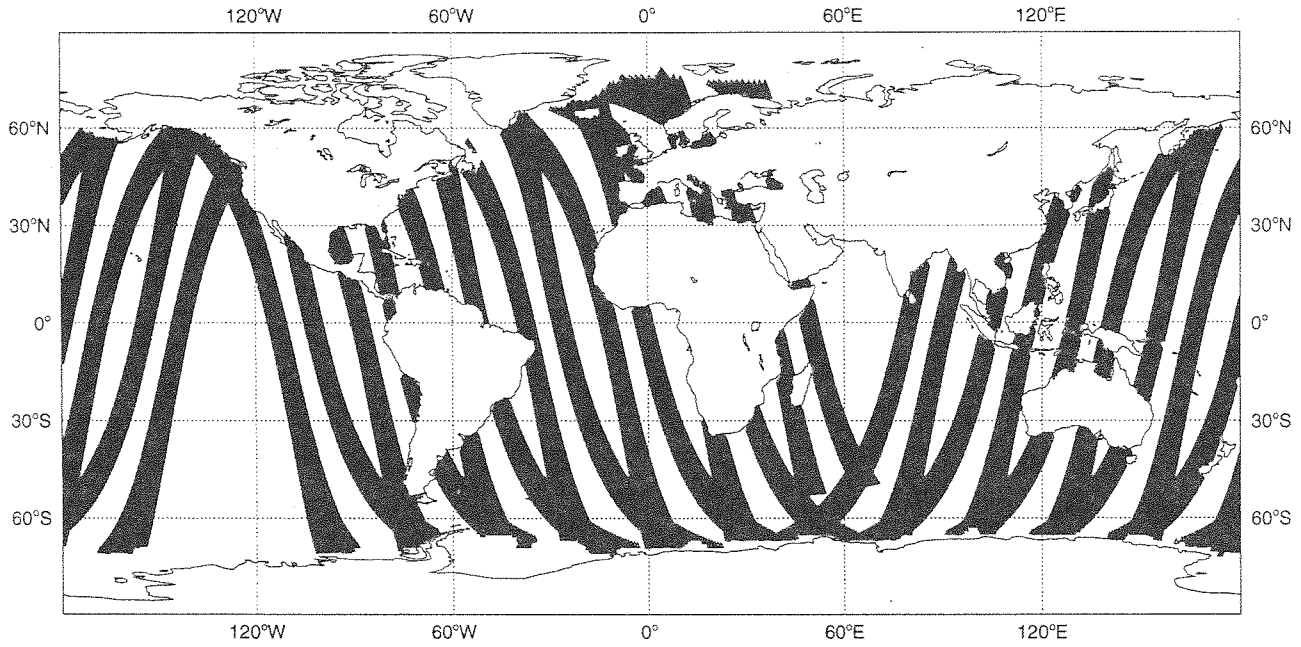

Fig 4.1: Simulated ASCAT data coverage on 26 February 1993 between 00 UT and 12 UT.

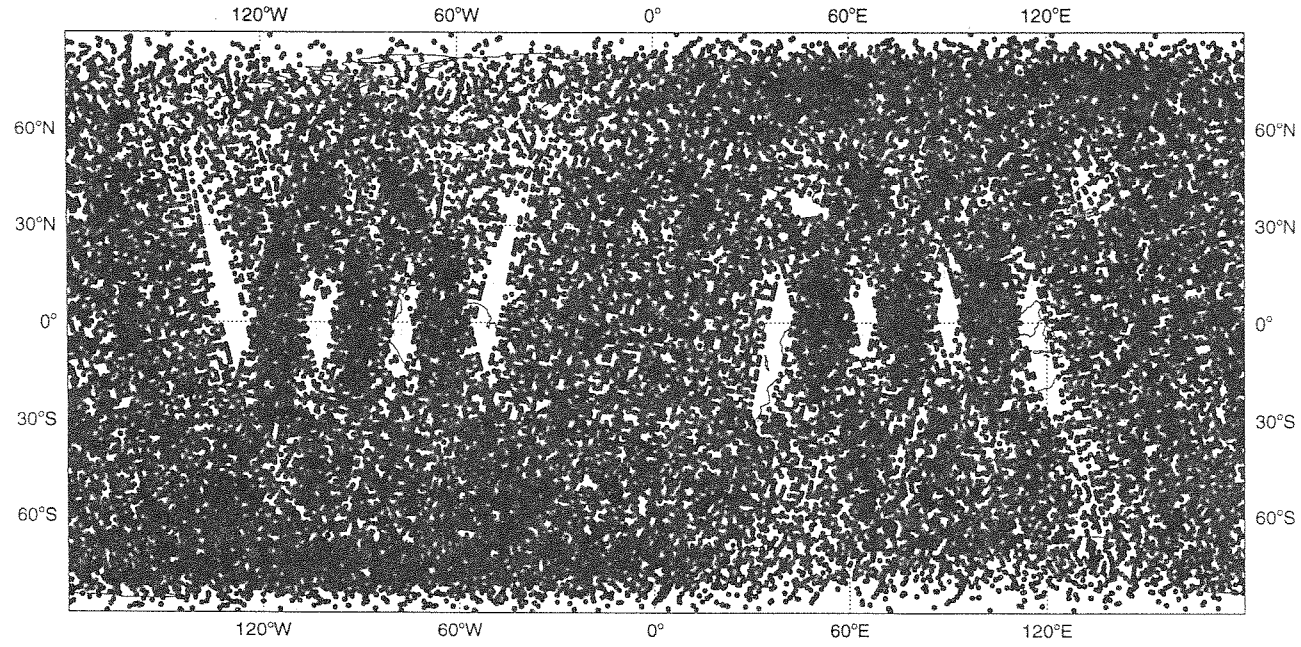

Fig 4.2: Simulated ATOVS data coverage on 26 February 1993 between 00 UT and 12 UT.

4.1.2 *ATOVS*

The ATOVS pre-processor uses exactly the TOVS orbit simulator developed for the first OSSE data base project. It imitates the current NOAA two-satellite system and the spatial distribution of the "120 km BUFR TOVS" products, distributed by NESDIS operationally (Figure 4.2). These products are generated for every 3x3 box of HIRS Field-Of-View (FOV), resulting in a scanning geometry of 18 boxes across-track with an angular spacing of 5.4 degrees, and a time between boxes along-track of 19.2 seconds. Finally, a random removal of 50% of the soundings is applied, to imitate their data selection process.

The TOVS pre-processor has been adapted to handle the 40 ATOVS channels (27 channels for TOVS) and to keep time information at an accuracy of one second, as for ASCAT data.

4.2 **Observation simulator**

4.2.1 *ASCAT*

In the 3D-VAR assimilation system currently under development at ECMWF (*Courtier et al*, 1993), ERS-1 backscatter measurements are not assimilated directly into the IFS, but as a pair of ambiguous 10-metre wind vectors, retrieved from backscatter measurements at a pre-processing stage. As a consequence, ASCAT backscatter measurements are not simulated directly by the observation simulator (IFS), which computes only a "true" 10-metre wind vector at the observation location. The corresponding backscatter measurements (σ_0's) are generated afterwards, by the post-processor. The 10-metre wind is deduced from wind at the lowest model level (32 m) by an appropriate interpolation, taking into account the physics of the surface boundary layer. An example of simulated 10-metre winds for ASCAT is given in Figure 4.3, on top of the corresponding model 10-metre wind field.

4.2.2 *ATOVS*

The development of the observation simulator for ATOVS required to integrate a new observation operator for radiative transfer into IFS, to compute the brightness temperatures for all AMSU and HIRS channels from model fields. This code was developed and scientifically validated (see for instance *Eyre and Woolf*, 1988 and *Eyre*, 1990) by extending the fast forward model called RTTOV, used for TOVS in the first project. A suitable interface with IFS was built to pass the needed

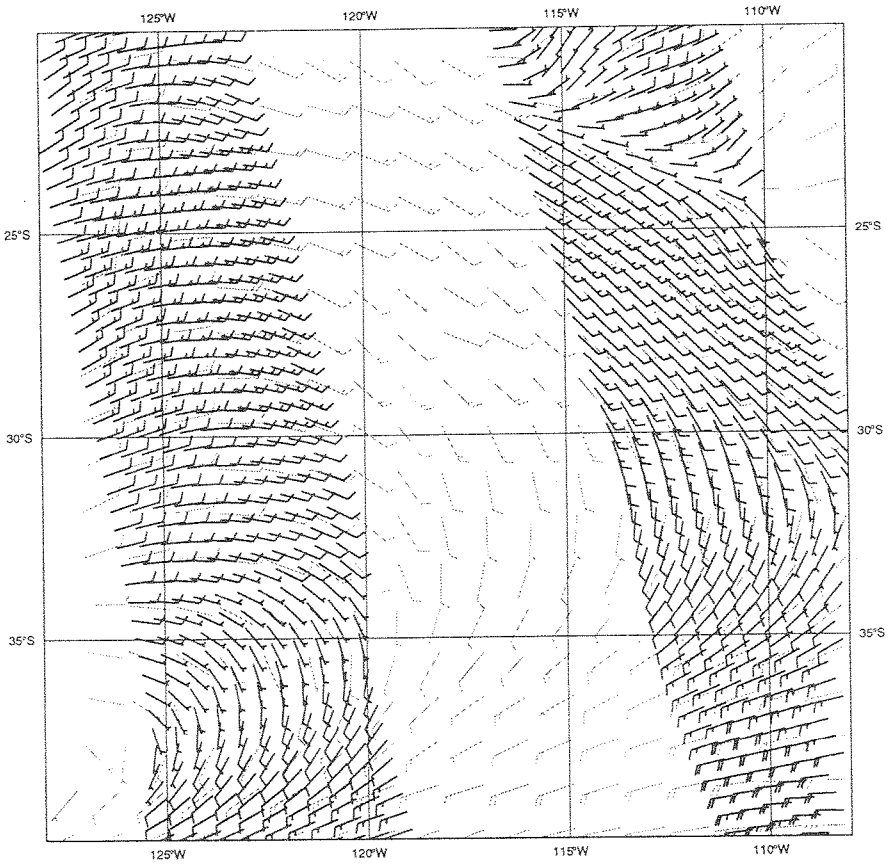

Fig 4.3: Example of simulated "true" ASCAT 10-metre winds on 9 February 1993 around 12 UT (dark), plotted on top of the corresponding IFS nature run field at 12 UT (light).

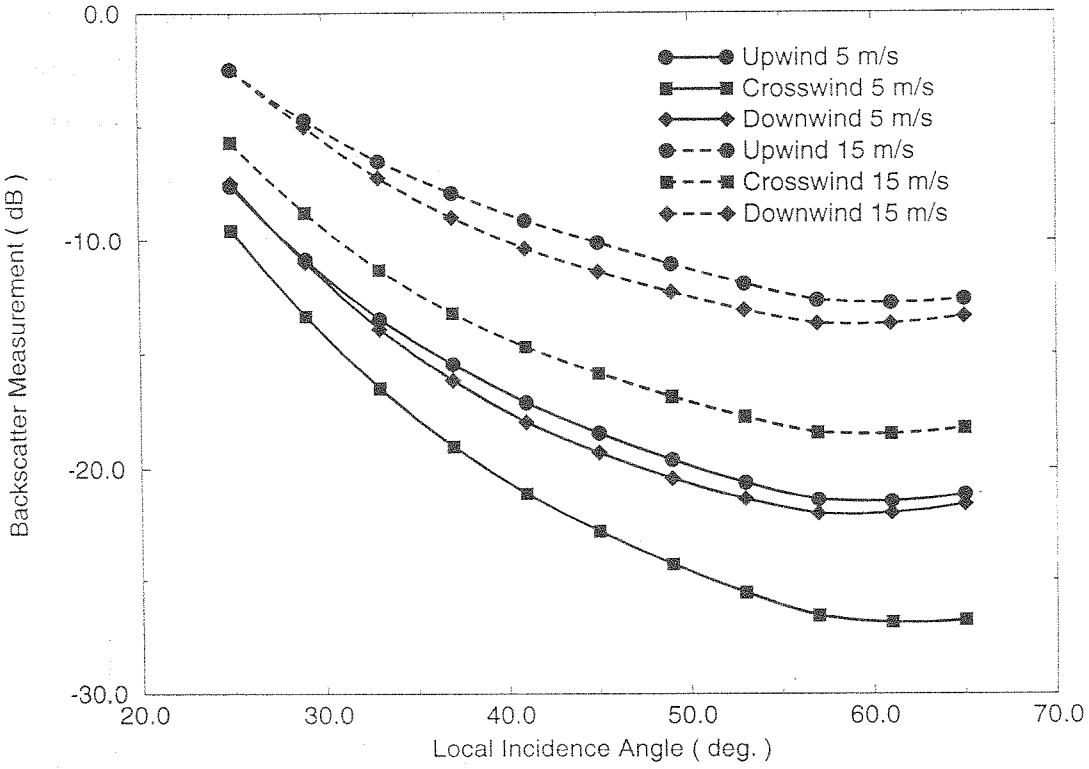

Fig 4.4: C-band backscatter values, computed from the CMOD4 transfer function for upwind, downwind and crosswind cases, and for 5 and 15 m/s wind speeds.

atmospheric and surface quantities from the model to the radiative transfer code, which returns brightness temperatures and total cloud cover to be saved in the CMA files. In particular, the fast forward model requires temperature and humidity profiles on a set of 40 fixed pressure levels. In the vertical domain of the IFS model, these profiles were interpolated linearly from the temperatures and humidities at model levels. However, the temperatures requested on the upper levels (from 5 to 0.1 hPa) were derived from the temperatures on lower levels, using a multilinear regression scheme. The details are given in Appendix A.

4.3 **Post-processor**

4.3.1 *ASCAT*

For ASCAT data, the observed quantity produced by the observation simulator is a 10-metre wind vector. As shown by *Stoffelen and Anderson* (1995) for ERS-1 scatterometer, the characteristics of scatterometer errors cannot be characterized entirely in terms of backscatter measurement errors because of the strong non-linearities in the transfer function, and because of representativeness errors. Following their results, we generated scatterometer errors in the following way:

- Add a gaussian error of 1.6 m/s standard deviation to each component of 10-metre wind vector before computing backscatter measurements (hereafter called σ_0's), to simulate both transfer function and representativeness errors.
- Add a gaussian error to the three computed σ_0's at a given node, to simulate the geophysical part of the σ_0 errors. Its standard deviation was set equal to 0.000644 $(V-16)^2$ σ_0, where V is the wind speed in m/s.
- Add an independent gaussian error to each of the three σ_0's, to simulate the instrumental (or detection) part of the σ_0 errors. Its standard deviation was set equal to 0.05 σ_0, which is a common value for the current ERS-1 backscatter measurements.

The "true" σ_0's were computed from a 10-metre wind vector using the CMOD4 transfer function, which was derived by *Stoffelen and Anderson* (1995) using ECMWF wind analyses, for ERS-1 backscatter measurements in C-band. The CMOD4 transfer function is given in Appendix B. CMOD4 was extrapolated for incidence angles up to 62.5°, to suit the ASCAT/METOP configuration. Figure 4.4 shows the upwind, downwind and crosswind backscatter values derived from CMOD4 for incidence angles between 25° and 65°. A change of the derivative sign occurs around 60°, which

does not seem to be physically realistic. However, this problem does not affect the wind retrieval from simulated ASCAT backscatter measurements itself.

4.3.2 *ATOVS*

For ATOVS data, the procedure used to generate errors is very similar to the one used in the first project for TOVS data. Two different types of error are generated and applied independently for each channel:

- Gaussian errors, with a zero mean and a predefined standard deviation σ, depending on the channel and on the cloud cover for infra-red channels.
- Gross errors, which are drawn from a uniform distribution between $-R/2$ and $R/2$, where R is the gross error range (20° K whatever the case).

Gaussian and gross errors are alternatively generated, according to the probability P_G of gross error occurrence in the following way:

IF RANF() < PG
$T_B = T_B + G(0,\sigma)$
ELSE
$T_B = T_B + U(-R/2,R/2)$
ENDIF

For the HIRS channels, the generated errors have exactly the same characteristics as in the first project. They depend on the choice of the cloud-clearing route, based on the total fractional cloud cover N. To account for subgrid scale effects in the nature run cloud cover, a statistical decision algorithm is used, as illustrated in Figure 4.5. This algorithm has been tuned empirically, to match the average frequency of each cloud-clearing route in the operational NESDIS TOVS data set.

The values of σ used for the new ATOVS microwave channels have been assessed at 100 km resolution using the values from *Eyre* (1990). σ values include radiometric noise, pre-processing errors, radiative transfer modelling errors and representativeness errors, and are independent of cloud cover. The values of P_G have been set empirically for AMSU from the comparable HIRS and MSU channels. Both values are listed in Table 4.1.

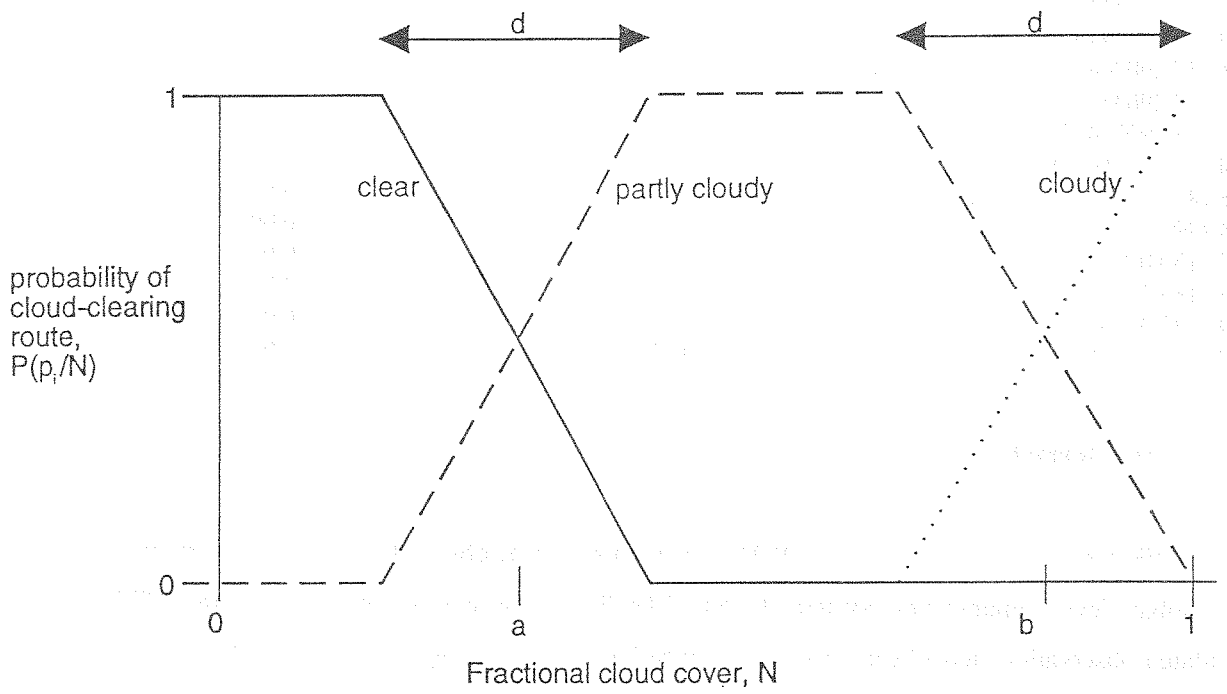

Fig 4.5: Illustrating the cloud-clearing route decision algorithm used for simulated TOVS and ATOVS data.

Table 4.1: ATOVS simulated standard deviation of error(σ) and probability of gross error(P_G) for the different AMSU simulated channels. The assumed gross error range is 20 K.

ATOVS channel	σ (K)	P_G
21 (23.8 GHz)	1.15	0.005
22 (31.4 GHz)	1.15	0.005
23 (50.3 GHz)	1.15	0.005
24 (52.8 GHz)	0.59	0.002
25 (53.596 GHz)	0.33	0.001
26 (54.4 GHz)	0.29	0.001
27 (54.94 GHz)	0.27	0.001
28 (55.5 GHz)	0.28	0.001
29 (57.290344 GHz)	0.28	0.001
30 (57.290344 GHz)	0.32	0.001
31 (57.290344 GHz)	0.32	0.002
32 (57.290344 GHz)	0.40	0.003
33 (57.290344 GHz)	0.50	0.004
34 (57.290344 GHz)	0.76	0.005
35 (89.0 GHz)	1.14	0.005
36 (89.0 GHz)	1.14	0.005
37 (150.0 GHz)	1.14	0.005
38 (183.31 GHz)	1.52	0.002
39 (183.31 GHz)	1.05	0.002
40 (183.31 GHz)	0.75	0.002

4.4 **Bufr formats**

The BUFR format is recommended by WMO for the transfer of observational data, in particular on the Global Telecommunication System (GTS). The BUFR formats for the ASCAT and ATOVS simulated observations have been chosen as compatible as possible with the current BUFR formats of ERS-1 scatterometer and TOVS real observations transmitted on the GTS.

The BUFR format is a very flexible table-driven format, which allows any additional information needed to be appended to the main report in a standard way. This facility has been used extensively to store the following information:

- For ASCAT data, the "true" backscatter values derived from CMOD4 and the error standard deviations used in the backscatter noise generation.
- For ATOVS data, the "true" brightness temperatures from the nature run, the error standard deviations used in the gaussian error generation, the probabilities of gross error used in the gross error generation and the gross error indicator for each channel.

In addition, we stored in the main body of the ASCAT BUFR reports the 10-metre wind vector used in the σ_0 computation, and the missing packet number (Descriptor number 021195, see Appendix C) was used to store the node number of the observation in the swath (from -21 to -1 on port side and from 1 to 21 on starboard side).

5. VALIDATION

5.1 Observation simulator

The validation of the ASCAT observation simulator was rather straightforward, and was done by comparing the nature run 10-metre wind field with the values interpolated at ASCAT space and time locations. Such a comparison is shown in Figure 4.3.

For ATOVS, the outputs of the observation simulator were checked quantitatively against the TOVS brightness temperatures for the common infra-red channels (channels 1 to 20) simulated in the first project. For the microwave channels, we compared qualitatively the AMSU simulated brightness temperatures with the ones of the HIRS and MSU channels, which have similar weighting functions. These channels are given in Table 5.1.

Table 5.1: HIRS, MSU and AMSU channels, used for the validation of the ATOVS brightness temperatures.

Peak Energy Level	HIRS	MSU	AMSU
50 hPa (temp.)	channel 2	-	channel 10
100 hPa (temp.)	channel 3	channel 4	channel 9
300 hPa (temp.)	-	channel 3	channel 7
600 hPa (temp.)	channel 5	channel 2	channel 5
Surface (temp.)	-	channel 1	channel 3
700 hPa (hum.)	channel 11	-	channel 19

Figures 5.1 a) and b) illustrate these comparisons for MSU channel 4 and AMSU channel 9. In these plots, the simulated brightness temperatures on 5 February 1993 between 05 and 08 UT are plotted using the colour scale given on top of the plot and are superimposed with the nature run temperature field at 06 UT, at 100 hPa. Figures 5.2 a) and b) are the same as Figures 5.1 a) and b), but for MSU channel 1 and AMSU channel 3, superimposed with 1000 hPa temperatures.

5.2 Post-processor

Figure 5.3 shows statistics on the departures between "true" and noisy σ_0's as a function of wind speed, for a one day period and three different latitude bands. The light dotted curve is the mean of the applied errors on σ_0's (normalized by σ_0), which is always very close to zero, except for low counts (extreme high wind speeds). The light solid curve is the root mean square of the applied errors on σ_0's (normalized by σ_0), which exactly matches the theoretical error standard deviation (dark

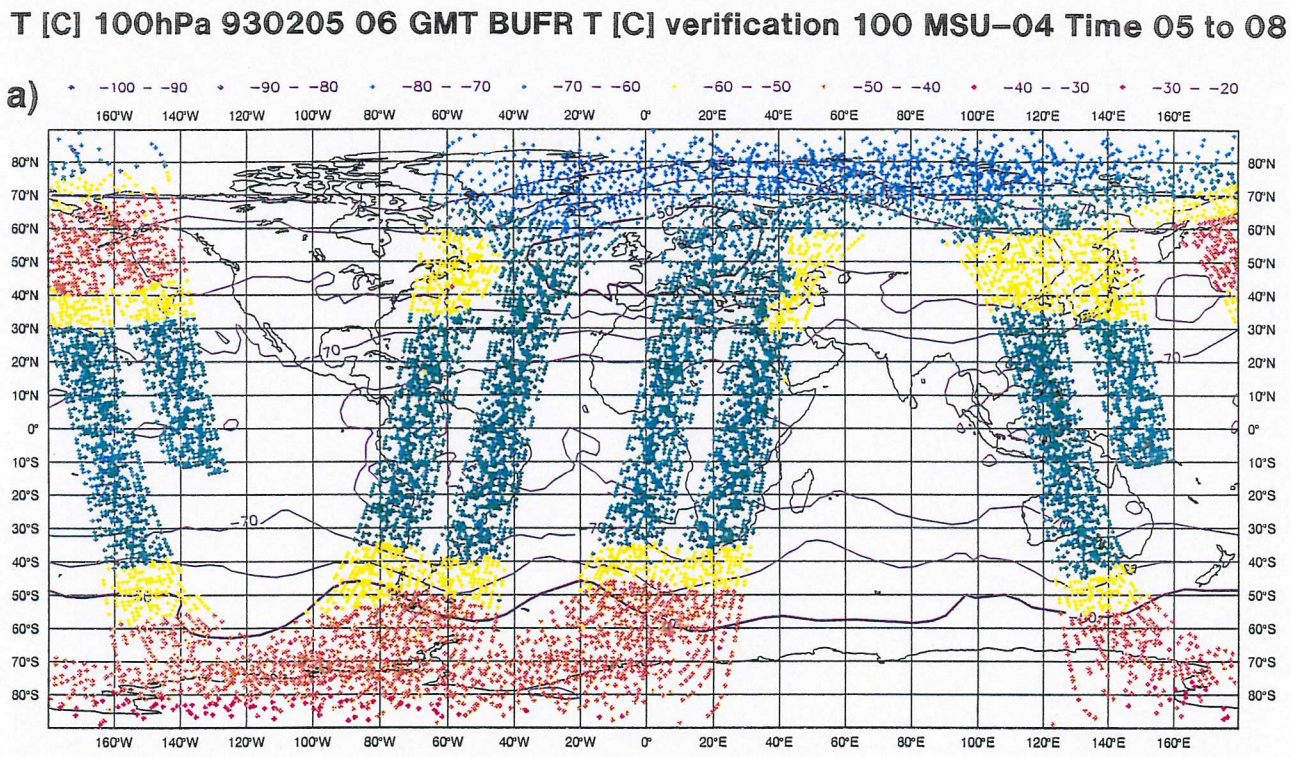

Fig. 5.1 a)

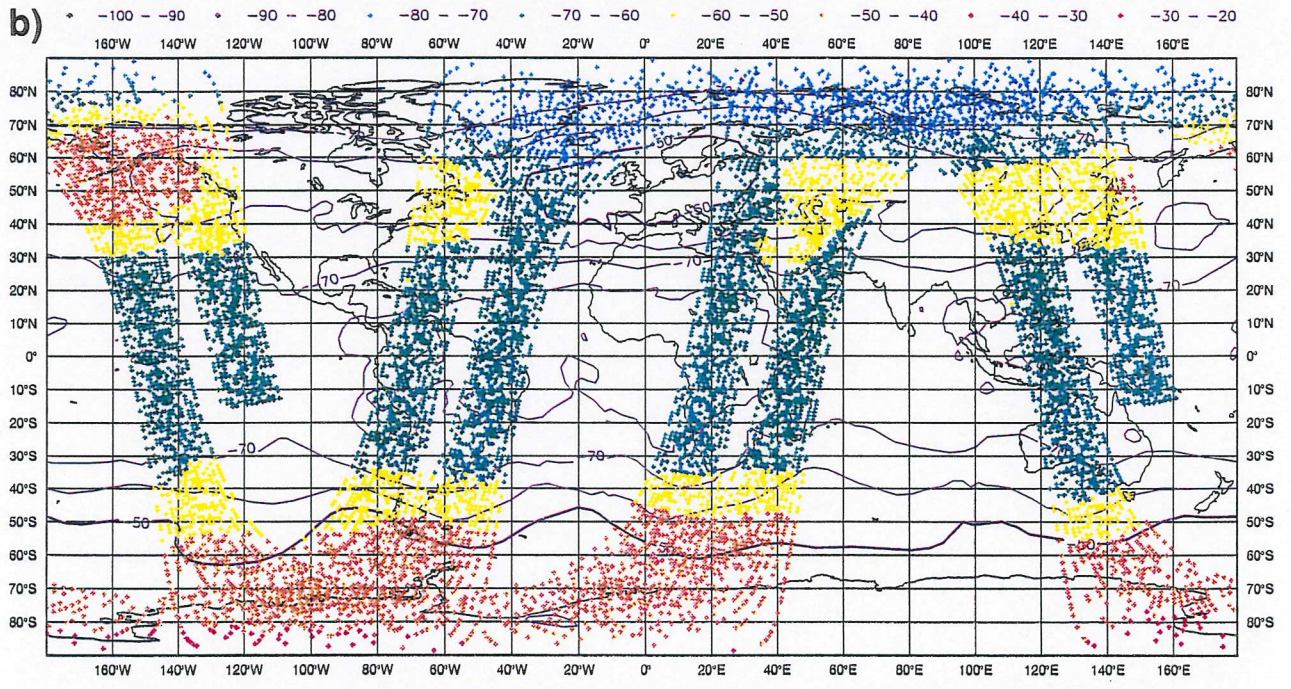

Fig 5.1: Simulated brightness temperatures of MSU channel 4 (a)) and AMSU channel 9 (b)), on 5 February 1993 between 05 and 08 UT. The colour scale is indicated on top of the plot and the background field is the nature run temperature at 100 hPa and 06 UT.

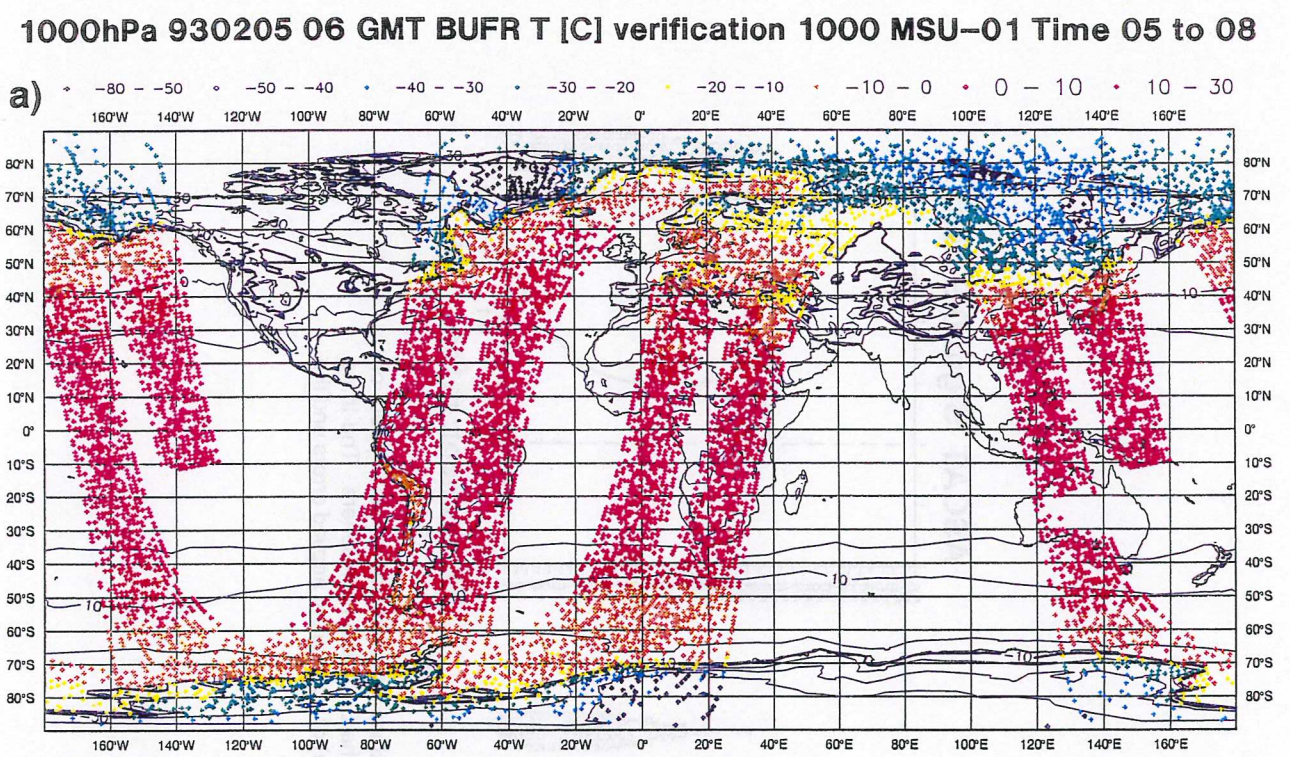

Fig. 5.2 a)

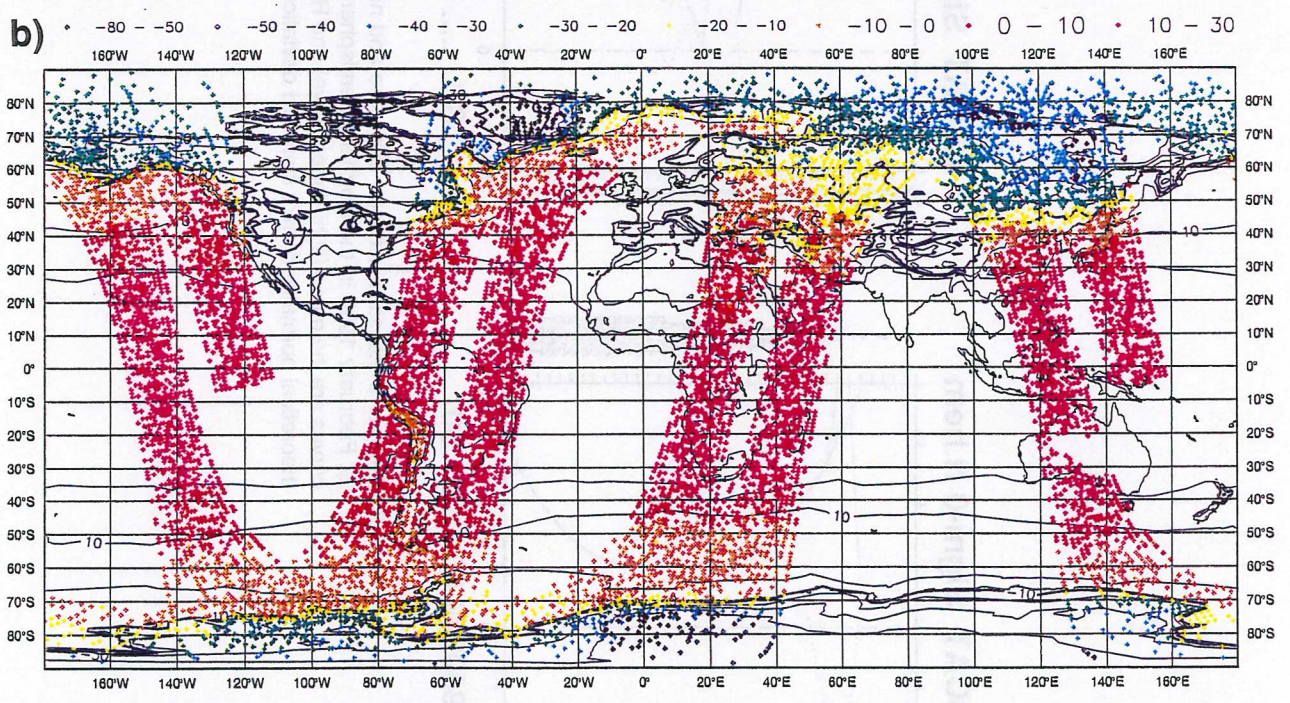

Fig 5.2: Same as Figure 5.1, but for MSU channel 1 (a)) and AMSU channel 3 (b)). The background field is the nature run temperature at 1000 hPa.

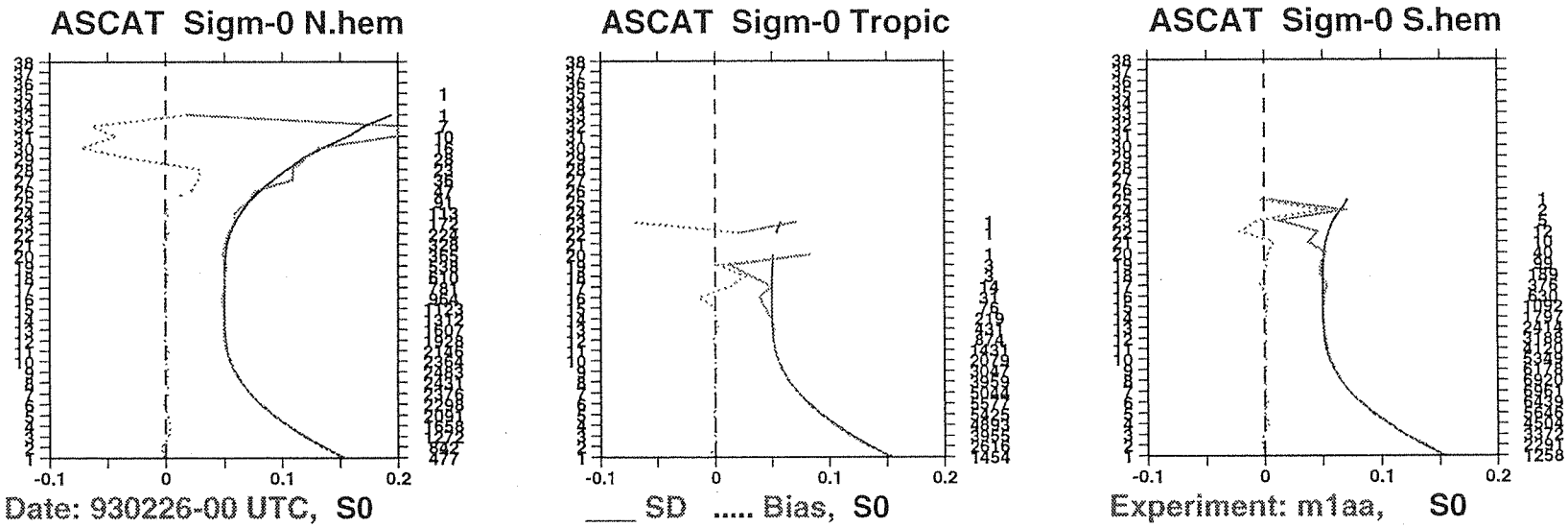

Fig 5.3: Departure statistics between error-free and noisy simulated σ_0 values as a function of wind speed, on 22 February 1993 in the Northern Hemisphere, the Tropics and the Southern Hemisphere. The three curves are the mean (light dotted curve) and RMS (light solid curve) of normalized applied errors and the theoretical normalized error standard deviation (dark solid curve).

solid curve). This plot also verifies that the minimal backscatter errors occur for a wind speed of 16 m/s, with a minimum value of 5%.

Figure 5.4 shows the departure statistics for a one day period between the error-free and the noisy brightness temperatures with gaussian errors only for the forty ATOVS channels. The results are shown for the first satellite (NOAA 11) over sea (upper plots) and over land (lower plots). From left to right, the different plots are for clear, mixed and cloudy conditions respectively and display mean (light dotted curve) and root mean square (light solid curve) of the applied errors. Mean is always close to zero and root mean square perfectly matches the theoretical error standard deviation (dark solid curve). Figure 5.5 is the same as Figure 5.4, but for gross errors only. The match is less good, just because of the much lower counts, indicated on the right-hand side of the plots.

5.3 **Final Data base**

5.3.1 *ASCAT*

The ASCAT backscatter measurements were validated by comparing retrieved and input wind vectors to the CMOD4 transfer function. We used a new retrieval module, developed at ECMWF for ERS-1 backscatter measurements, which was interfaced to the new ASCAT BUFR products. This module looks after the multiple minima of a cost function, measuring the departures between the observed and retrieved σ_0's for the 3 antennae, and does not need any background wind information. The cost function is computed using a CMOD4 transfer function table, discretized for 0.5 m/s wind speed and 5° wind direction intervals. Then, to assess and validate the impact of our σ_0 noise generation procedure independently of any ambiguity removal procedure, we selected the retrieved wind vector, which was the closest to the initial one in terms of direction.

Figure 5.6 shows the departure statistics between the input and retrieved wind speeds and directions, as a function of node number on 5 February 1993 (127402 wind vectors). Note that for a 25 km horizontal sampling, the ASCAT swath consists of 21 nodes, but in the present data base ASCAT measurements were simulated with a 50 km horizontal sampling. The mean wind speed and direction differences are very close to zero and the difference standard deviations decrease towards the end of the swath, with values ranging from 0.38 to 0.29 m/s (respectively from 4.6 to 2.9°) for wind speed (respectively direction). These values agree very well with the ones obtained by *Stoffelen and Anderson* (1993) for ERS-1 simulated backscatter measurements.

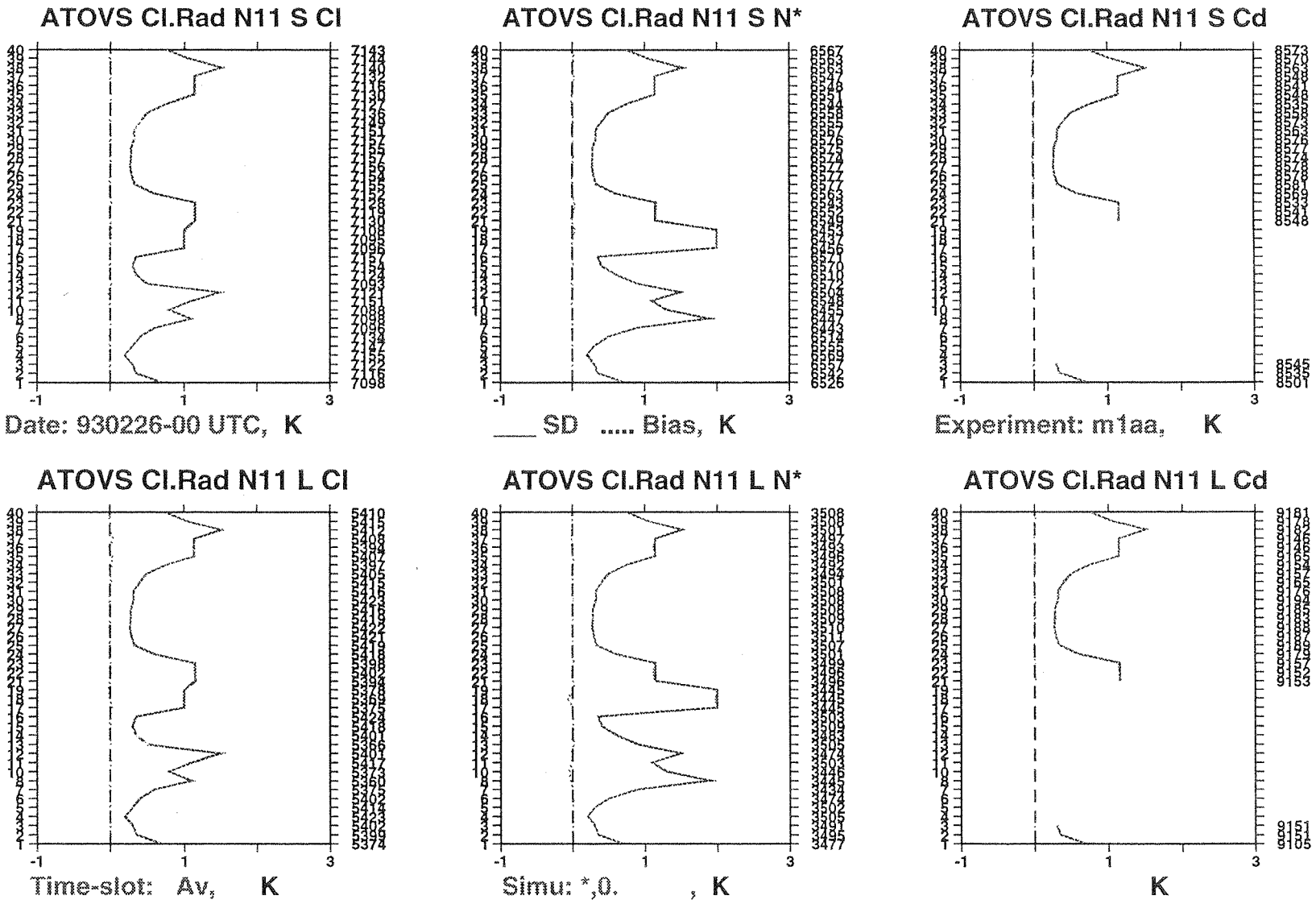

Fig 5.4: Departure statistics between error-free and noisy simulated ATOVS brightness temperatures as a function of channel for the first satellite, on 22 February 1993 over sea and over land, and for clear, mixed and cloudy conditions. The three curves are the mean (light dotted curve) and RMS (light solid curve) of applied errors, and the theoretical error standard deviation (dark solid curve), for gaussian errors only.

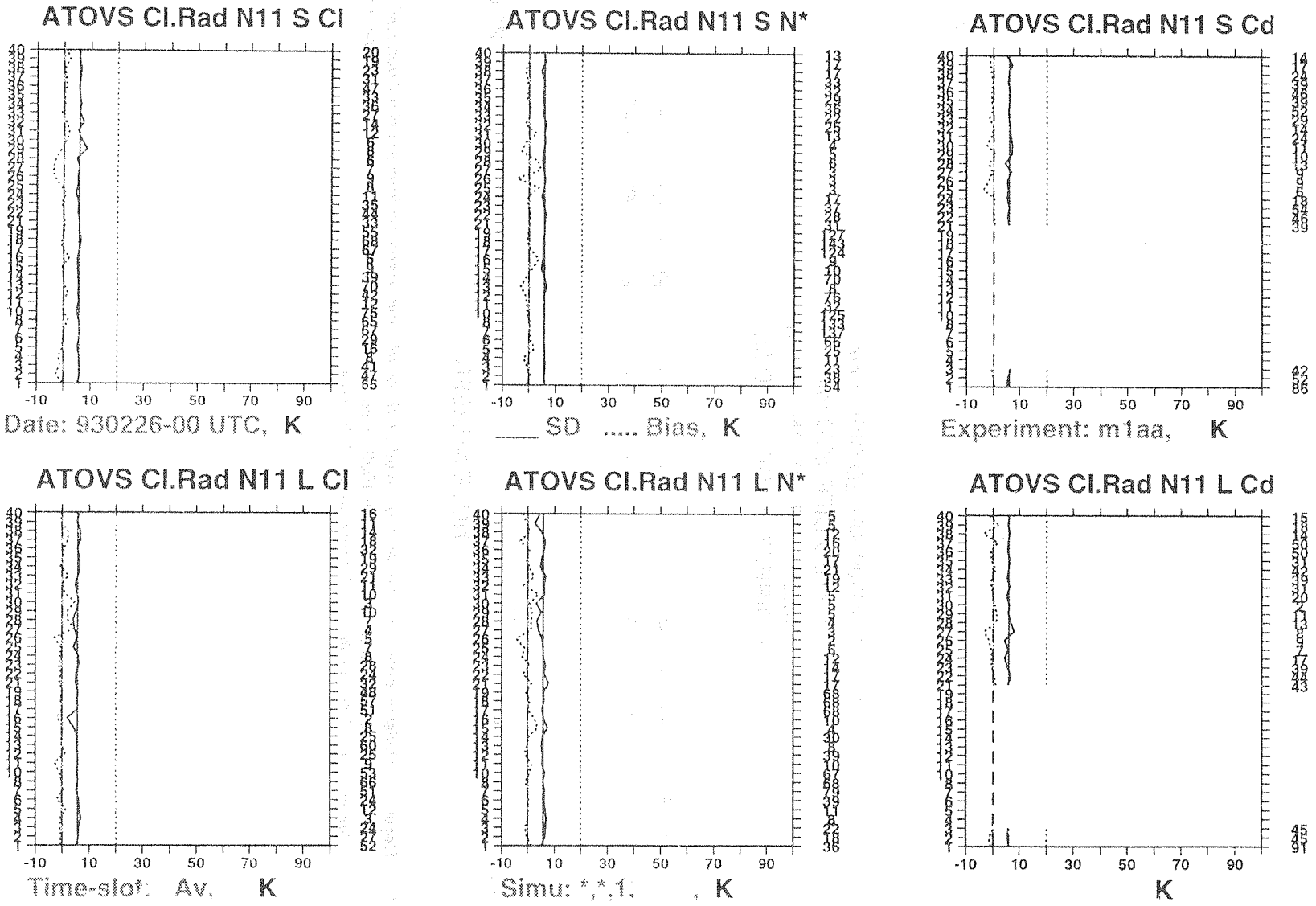

Fig 5.5: Same as Figure 5.4, but for gross errors only. The different curves are the mean (dark dotted curve) and RMS (dark solid curve) of applied error, the theoretical error standard deviation (light solid curve) and the gross error range (light dotted curve).

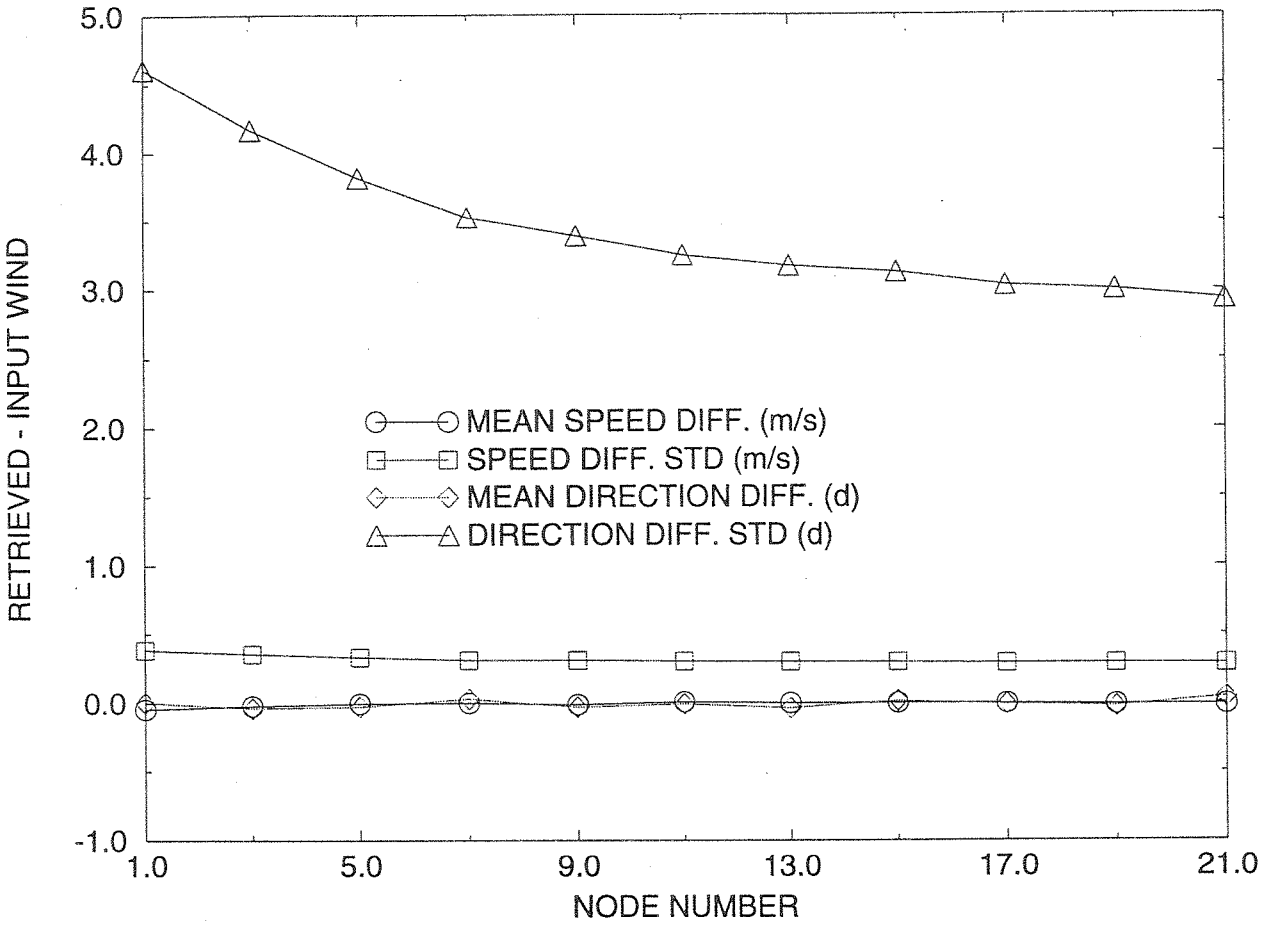

Fig 5.6: Departure statistics between input and retrieved wind speeds and directions from the simulated ASCAT backscatter measurements, on 5 February 1993. They are plotted as a function of the node number from 1 (inner edge of the swath) to 19 (outer edge of the swath).

5.3.2 *ATOVS*

Since the development of a new retrieval system for ATOVS measurements is a full scientific task in itself, out of the scope of this project only the TOVS brightness temperatures (i.e. the HIRS, MSU and SSU ones) were inverted using the PRESAT procedure, which is operational at ECMWF. The retrieval method is presented for instance in *Eyre* (1990), and relies on the minimization of the following cost function:

$$J(x) = \tfrac{1}{2} (x - x^b)^T C^{-1} (x - x^b) + \tfrac{1}{2} \{ y^m - y(x) \}^T (E + F)^{-1} \{ y^m - y(x) \}$$

where:

x is the vector containing the retrieved temperature and humidity profile

C is the expected covariance of background error

x^b is the background profile

y^m is the vector of measured brightness temperatures

E is the expected covariance of measurement error

$y(x)$ is the radiative transfer model estimating the brightness temperatures from x

F is the expected covariance of forward model error.

The use of a background profile is necessary in the retrieval procedure as the atmospheric profile corresponding to a given set of TOVS brightness temperatures is not unique. Note that at the present temperature it is only retrieved up to 50 hPa and humidity up to 300 hPa. For our validation purposes we used the nature run fields archived 6-hourly as background fields.

In Figures 5.7 (respectively 5.8) the departure statistics between retrieved and background temperature (respectively humidity) on 5 February 1993 between 03 and 09 UT, are plotted against pressure level for the Northern Hemisphere (a)), the Tropics (b)) and the Southern Hemisphere (c)). The following error sources contribute to these departures:

- The gaussian and gross errors, applied on the brightness temperatures at the post-processing stage.
- The errors due to the retrieval procedure.
- The evolution of the nature run atmospheric fields which the brightness temperatures were computed from, within the 6-hour time interval.

For retrieved humidity profiles, the mean departures from background profiles are very close to zero and the standard deviations increase from about 0.1 (units: Log of g/kg) at 1000 hPa to about 0.2 at 300 hPa. For retrieved temperatures, a very slight positive bias is present in the troposphere, in particular in the Tropics (around 0.03° C). However, this feature is not present for other time periods. The standard deviations have a maximum at 250-200 hPa, corresponding also to maximal background

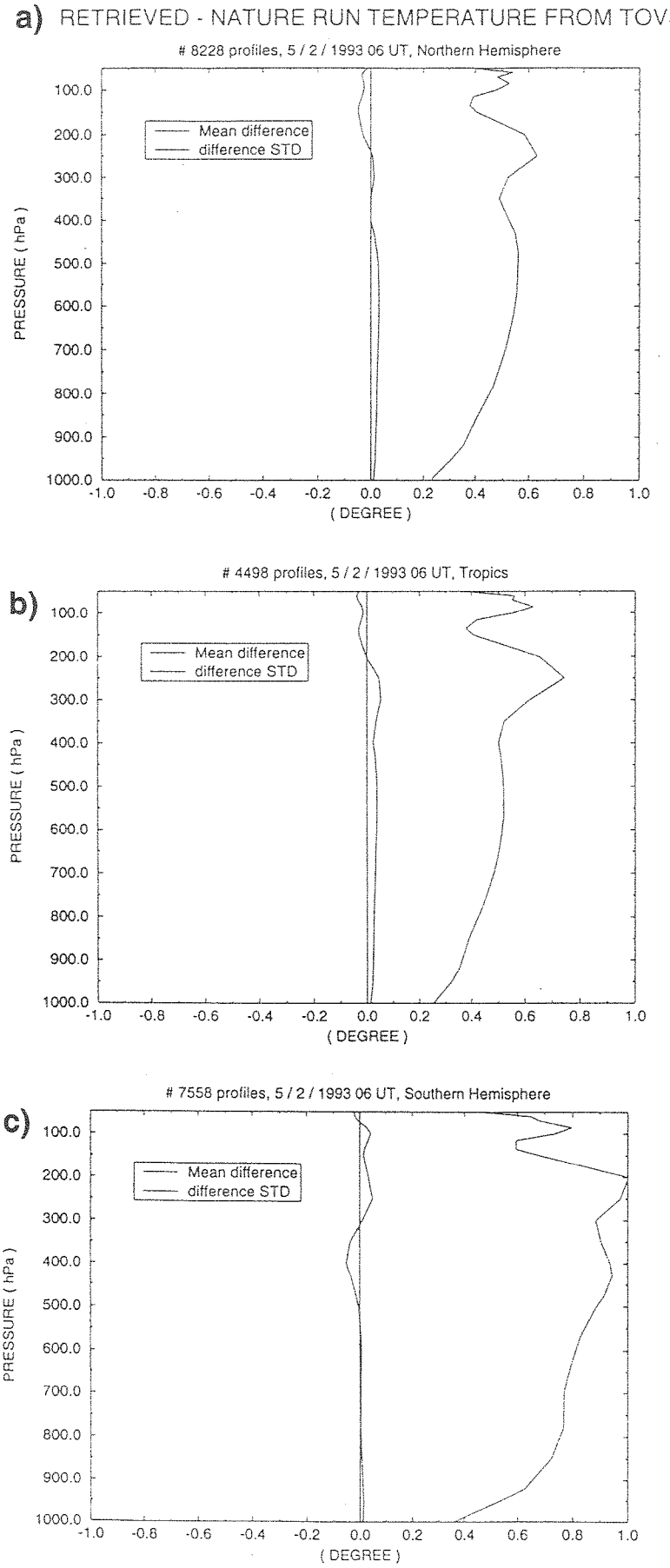

Fig 5.7: Departure statistics between nature run and retrieved temperatures from TOVS brightness temperatures, on 5 February 1993 between 03 and 09 UT using the PRESAT procedure. They are plotted as a function of pressure level for the Northern Hemisphere (a)), the Tropics (b)) and the Southern Hemisphere (c)).

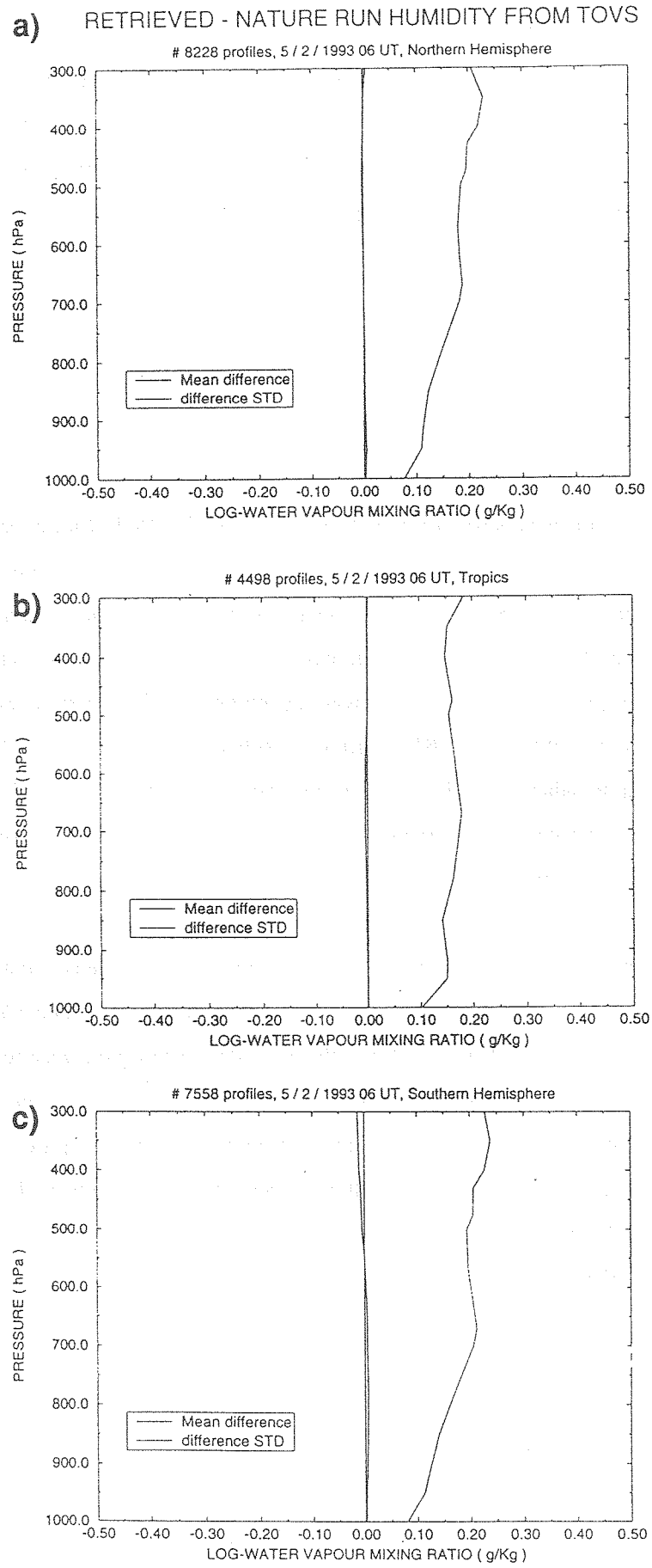

Fig 5.8: Same as Figure 5.7, but for nature run and retrieved humidity.

error standard deviations in PRESAT (see *Eyre*, 1990). They are larger in the Southern than in the Northern Hemisphere whatever the pressure level (difference Southern minus Northern Hemisphere of about 0.4° C around 500 hPa). This difference is due to the cloud cover, which is larger in the nature run during this period in the Southern than in the Northern Hemisphere and which leads to larger error standard deviations and gross error probabilities in the post-processing of the simulated brightness temperatures. PRESAT was also applied on error-free brightness temperatures from the nature run and, in this case, no significant difference between Southern and Northern Hemisphere was found.

5.3.3 *Assimilation experiment*

A short assimilation experiment was performed within the current ECMWF Optimal Interpolation (OI) and 3D-VAR systems, as an overall validation of the whole OSSE data base. This experiment was run at spectral truncation T106 (equivalent horizontal resolution $\approx$ 150 km), assimilating all the simulated observations usable in the current operational system (conventional observations plus TOVS brightness temperatures), without any major software development. However, a few developments were necessary to sort the OSSE daily BUFR files for 6-hour time periods and for the different observation types, and to adapt the PRESAT pre-processing procedure to the TOVS simulated brightness temperatures. A parallel experiment was run using real observations, in particular to check the simulated observation coverage and rejections.

This final validation proved to be very useful, since it enabled us to detect and to correct two problems in the first OSSE data base, in the AIREPs vertical locations and land SYNOPs pressure observations. After corrections of these problems, the assimilation test gave very realistic results in terms of observation quality control, analysed fields and departures from observations before and after the analysis step. An illustration of the assimilation experiment is given in Figure 5.9 a), where the rejected pressure and wind observations are plotted on top of the sea pressure field from the OI analysis on 5 February 1993 at 06 UT, in the Southern Hemisphere. Figure 5.9 b) is the same as Figure 5.9 a), but assimilating real observations.

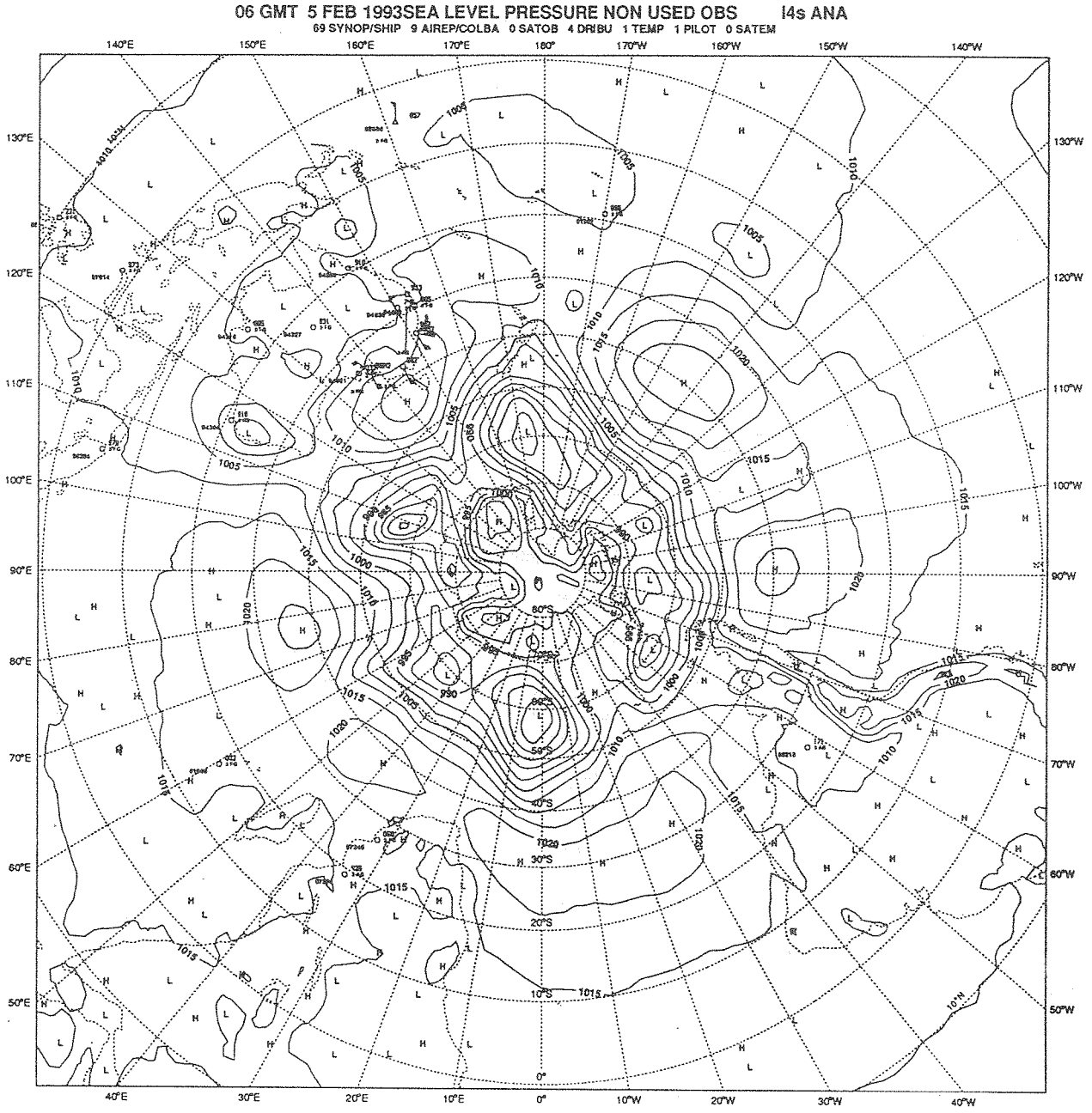

Fig 5.9: Analysed sea level pressure field (hPa) on 5 February 1993 at 06 UT in the Southern Hemisphere, assimilating simulated (a)) and real (b)) observations. The analysis was produced by the ECMWF Optimal Interpolation (OI) scheme, and the rejected wind and pressure observations are plotted on top.

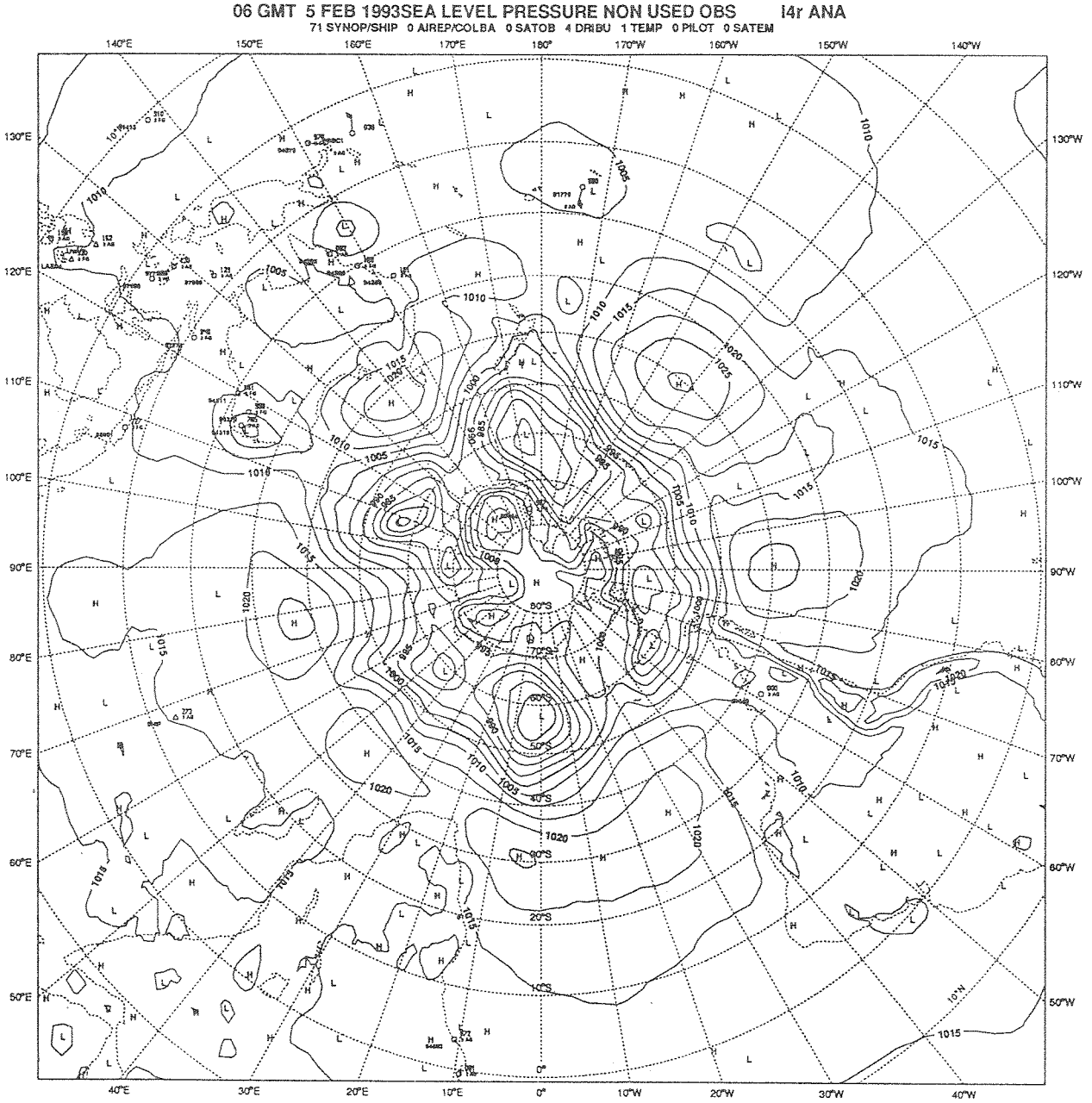
06 GMT 5 FEB 1993SEA LEVEL PRESSURE NON USED OBS I4r ANA
71 SYNOP/SHIP 0 AIREP/COLBA 0 SATOB 4 DRIBU 1 TEMP 0 PILOT 0 SATEM

Fig. 5.9 b)

6. CONCLUDING REMARKS

At present, the instrument which offers the best prospect for providing global, three-dimensional wind observations is the space-borne Doppler Wind Lidar (DWL). However, such a space-based system implies advanced technical requirements, and its development will be long and costly. Therefore, realistic simulated DWL Line-Of-Sight (LOS) wind measurements can be very useful to study their sensitivity to instrument and orbit characteristics in terms of quality and distribution, and to assess their usefulness for Numerical Weather Prediction (NWP) through Observing System Simulation Experiments (OSSE).

In a previous ESA-funded project, a 30-day data base of simulated observations was produced at ECMWF, including conventional observations, TOVS cloud-cleared brightness temperatures from two NOAA-like satellites and DWL LOS wind measurements for four different instrument and orbit scenarios. However, realistic OSSEs have to take into account the new instruments, which are known to be flown soon by the next meteorological operational satellites. Therefore, the objective of the present project was to extend the existing data base, to Advanced SCATterometer (ASCAT) and Advanced TOVS (ATOVS) measurements, simulated fully consistently with the previous observations. Note that the proposed high spectral resolution infra-red interferometer, which is also planned to be launched on METOP, has not yet been simulated. Data from this instrument will improve the vertical resolution of the temperature and humidity profiles.

The assumed true meteorological state, from which ASCAT and ATOVS measurements were simulated, was provided by a 30-day run of the ECMWF IFS model, with a T213 spectral truncation (equivalent horizontal resolution $\approx$ 80 km) and 31 vertical levels. The model was used exactly in the same version and initialized from the same operational analysis as in the previous project. The ASCAT backscatter measurements were computed from the IFS 10-metre winds, using a transfer function (CMOD4) and an error generation procedure, derived from ERS-1 backscatter measurements. The ATOVS cloud-cleared brightness temperatures were computed directly within the IFS model, using a fast radiative transfer model, adapted for the new ATOVS microwave channels.

A lot of tests have been performed to validate each element of the production chain and also the final BUFR products. 10-metre winds have been systematically retrieved from the simulated ASCAT backscatter measurements and compared to the initial winds. No tool was available to fully validate simulated ATOVS brightness temperatures, but we retrieved temperature and humidity profiles from TOVS brightness temperatures, hence indirectly validating the ATOVS infra-red brightness

temperatures. Finally, an assimilation experiment was performed using simulated conventional and TOVS data. This test proved to be very useful, as the ECMWF quality control of observations revealed problems in the simulated AIREP and SYNOP observations, which were corrected.

NWP centres can now make use of a comprehensive set of simulated observations, which should be very useful to assess the respective contribution of each observing system, including DWL LOS wind measurements. This data base can be also very useful for NWP centres to prepare for the coming of ATOVS and ASCAT measurements. The use of the data base was made very flexible, as BUFR products also contain the "true" (i.e. zero noise) observations, as well as the statistics used for the error generation. In that respect, the data base may also be a very good tool to study the ability of assimilation schemes to filter out observation errors of known characteristics and see whether systematic analysis errors develop during assimilation.

During the first project, the development at ECMWF of the production chain to simulate conventional, TOVS and DWL observations was a very demanding task, in particular from the computer resources and data handling point of view. This second project proved that this existing tool was working well and easy to adapt to simulate new observation types, such as ASCAT or ATOVS. This facility, which now exists at ECMWF, should also be very useful to prepare for radically new satellite instruments, such as for instance the European Infra-red Atmospheric Sounding Interferometer (IASI), which is also proposed to be on METOP.

Acknowledgements

We wish to thank J Eyre (UK Met Office), who provided the fast radiative model for the ATOVS channels, and A Stoffelen (KNMI), who assisted us for the generation of backscatter measurements errors. We are also thankful to C Gaffard (ECMWF), who provided the retrieval procedure for scatterometer winds, A McNally (ECMWF) for his assistance to use the PRESAT procedure and E Andersson and G Kelly (ECMWF) for answering our numerous questions about the assimilation system.

References

Courtier, P et al, 1993: Variational assimilation at ECMWF, ECMWF Tech Mem 194.

Eyre, J and H Woolf, 1988: Transmittance of atmospheric gases in the microwave region: a fast model, Appl Optics 27, pp 3244-3249.

Eyre, J, 1990: The information content of data from satellite sounding systems: a simulation study, QJRMS 116, pp 401-434.

Eyre, J, 1991: A fast radiative transfer model for satellite sounding systems, ECMWF Tech Mem 176.

Eyre, J, G Kelly, A McNally, E Andersson and A Persson, 1993: Assimilation of TOVS radiance information through one-dimensional variational assimilation, QJRMS 119, pp 1427-1463.

Saunders, R, S English and D Jones, 1994: AMSU-B: a new tool for atmospheric research, Proceedings of EUROPTO Series, Microwave Instrumentation and Satellite Photogrammetry for Remote Sensing of the Earth, 28-30 September 1994, Rome, Italy, SPIE Vol 2313 pp 98-107.

Stoffelen, A and D Anderson, 1993: Characterisation of ERS-1 scatterometer measurements and wind retrieval, in proceedings of the second ERS-1 Symposium held in Hamburg, Germany, 11-13 October 1993, ESA publication.

Stoffelen, A and D Anderson, 1995: The ECMWF contribution to the characterization, interpretation, calibration and validation of ERS-1 scatterometer backscatter measurements and winds, and their use in numerical weather prediction models, ESA CONTRACT REPORT.

Stoffelen, A, B Becker, J Eyre and H Roquet, 1994: Theoretical studies of the Impact of Doppler Wind LIDAR data. Preparation of a data base, ESA CONTRACT REPORT.

APPENDIX A: EXTRAPOLATION OF TEMPERATURE ABOVE 7 hPa

Inside IFS, the RTTOV radiative code requests the temperature at the following forty pressure levels to compute the cloud-cleared brightness temperatures: 0.1, 0.2, 0.5, 1, 1.5, 2, 3, 4, 5, 7, 10, 15, 20, 25, 30, 50, 60, 70, 85, 100, 115, 135, 150, 200, 250, 300, 350, 400, 430, 475, 500, 570, 620, 670, 700, 780, 850, 920, 950 and 1000 hPa.

Below 7 hPa, the temperatures are interpolated from the temperatures on the IFS model levels, linearly in logarithm of pressure. However, above 5 hPa the temperatures cannot be interpolated any more from the IFS temperatures and are extrapolated using a multilinear regression scheme. Each temperature from 5 hPa upwards is related to the temperatures on the 19 RTTOV pressure levels from 7 hPa to 400 hPa, with coefficients which were statistically derived from radiosonde data. Each temperature T_i (i=1, 9) from 0.1 to 5 hPa is computed according to:

$$T_i = \sum_{j=1}^{19} a_{i,j} T_j + b_i$$

with T_j (j=1, 19) temperature at level j from 7 to 400 hPa (T_i and T_j in Kelvin). The coefficients $a_{i,j}$ and b_i are listed in the following tables.

Table A.1: Regression coefficients used to extrapolate temperature to pressure levels from 0.1 to 5 hPa.

P (hPa)	0.1	0.2	0.5	1	1.5	2	3	4	5
7	-0.62913	-0.15991	0.54060	1.19776	1.34894	1.45516	1.41709	1.25330	1.12760
10	-0.13048	-0.16516	-0.21656	-0.27588	-0.22411	-0.18731	-0.08779	-0.02232	0.02760
15	0.20441	0.08097	-0.10450	-0.31957	-0.26198	-0.22138	-0.19312	-0.10249	-0.03200
20	0.43728	0.25354	-0.02323	-0.34533	-0.28429	-0.24144	-0.26416	-0.15606	-0.07129
25	0.13200	0.07375	-0.01919	-0.09831	-0.15691	-0.19753	-0.17970	-0.12984	-0.09162
30	-0.12581	-0.07623	-0.01139	0.11623	-0.04430	-0.15601	-0.10528	-0.10518	-0.10672
50	0.11273	-0.07274	-0.29303	-0.11030	-0.07342	-0.04908	0.11471	0.08556	0.06290
60	-0.05935	-0.05143	-0.03957	-0.03141	-0.02811	-0.02579	-0.03081	-0.03298	-0.03475
70	-0.20591	-0.03313	0.17684	0.03823	0.01232	-0.00456	-0.15275	-0.13264	-0.11715
85	-0.14863	-0.06637	0.03934	0.02960	0.01280	0.00160	-0.02094	-0.01699	-0.01433
100	-0.10180	-0.09441	-0.07457	0.02590	0.01600	0.00905	0.09185	0.08173	0.07323
115	0.01378	0.03260	0.06402	0.13083	0.11352	0.10126	0.10932	0.08473	0.06569
135	0.14758	0.18128	0.22806	0.25470	0.22708	0.20745	0.12787	0.08655	0.05535
150	0.23804	0.28012	0.33516	0.33554	0.30126	0.27686	0.14041	0.08802	0.04876
200	0.39087	0.30587	0.18882	0.05888	0.08045	0.09427	0.07644	0.01485	-0.03170
250	-0.36568	-0.23855	-0.05887	0.05838	0.08730	0.10823	0.04253	0.04679	0.04997
300	0.23959	0.13203	-0.02343	-0.08924	-0.13349	-0.16443	-0.14043	-0.09343	-005704
350	0.06203	0.10445	0.16586	0.22538	0.19008	0.16510	0.10212	0.05762	0.02363
400	-0.08270	0.08613	0.32963	0.48819	0.45974	0.43931	0.30089	0.17961	0.08657

Table A.2: Additive constants used to extrapolate temperature to pressure levels from 0.1 to 7 hPa.

0.1	0.2	0.5	1	1.5	2	3	4	5
221.9377	125.9144	-14.0449	-129.8705	-125.9651	-123.4266	-70.3035	-36.94878	-11.7851

APPENDIX B: THE CMOD4 MODEL FORMULATION AND COEFFICIENTS

The form of the ECMWF CMOD4 model is:

$$\sigma^0_{lin} = b_0.(1+b_1 \cos\phi+b_3 \tanh b_2.\cos 2\phi)^{1.6}$$

where: $b_0 = b_r.10^{\alpha+\gamma.f_1(V+\beta)}$

and $$f_1(y) = \begin{cases} 0 & if\ y \le 0 \\ \log y & if\ 0 < y \le 5 \\ \sqrt{y}/3.2 & if\ y > 5 \end{cases}$$

and α, β, γ, b_1, b_2 and b_3 are expanded as Legendre polynomials to a total of 18 coefficients. b_r is a residual correction factor to b_0 and is given as a Look-Up Table (LUT) as a function of local incidence angle.

$$\alpha = c_1P_0 + C_2P_1 + c_3P_2$$

$$\gamma = c_4P_0 + c_5P_1 + c_6P_2$$

$$\beta = c_7P_0 + c_8P_1 + c_9P_2$$

$$b_1 = c_{10}P_0 + c_{11}.V + (c_{12}P_0+c_{13}.V) \cdot f_2(x)$$

$$b_2 = c_{14}P_0 + c_{15}.(1+P_1).V$$

$$b_3 = 0.42(1+c_{16}(c_{17}+x)(c_{18}+V))$$

$$b_r = LUT(\theta)$$

$$f_2(x) = \tanh\{+2.5(x+0.35)\} - 0.61(x+0.35)$$

where the Legendre polynomials are:

$$P_0 = 1 \quad P_1 = x \quad P_2 = (3x^2-1)/2 \text{ with } x = (\theta-40)/25.$$

V is the wind speed in ms^{-1}, ϕ the relative wind direction in degrees and θ the incidence angle in degrees.

CMOD4 coefficients		
Model		CMOD4
α	c_1	-2.301523
	c_2	-1.632686
	c_3	0.761210
γ	c_4	1.156619
	c_5	0.595955
	c_6	-0.293819
β	c_7	-1.015244
	c_8	0.342175
	c_9	-0.500786
b_1	c_{10}	0.014430
	c_{11}	0.002484
	c_{12}	0.074450
	c_{13}	0.004023
b_2	c_{14}	0.148810
	c_{15}	0.089286
b_3	c_{16}	-0.006667
	c_{17}	3,000000
	c_{18}	-10.00000

Residual factors for CMOD4					
θ^0	b_r	θ^0	b_r	θ^0	b_r
16	1.075	31	0.927	46	1.054
17	1.075	32	0.923	47	1.053
18	1.075	33	0.930	48	1.052
19	1.072	34	0.937	49	1.047
20	1.069	35	0.944	50	1.038
21	1.066	36	0.955	51	1.028
22	1.056	37	0.967	52	1.016
23	1.030	38	0.978	53	1.002
24	1.004	39	0.988	54	0.989
25	0.979	40	0.998	55	0.965
26	0.967	41	1.009	56	0.941
27	0.958	42	1.021	57	0.929
28	0.949	43	1.033	58	0.929
29	0.941	44	1.042	59	0.929
30	0.934	45	1.050	60	0.929

APPENDIX C : BUFR FORMATS

In the following, we give lists of expanded BUFR descriptors for the simulated ASCAT and ATOVS observations we BUFR-ized. The first part of the BUFR message is in a standard observation format and contains the simulated noisy data. We only provide data for the relevant descriptors and descriptors that we consider irrelevant are always set to missing. The second part describes ancillary variables and the "true" observed variables and set up a backward reference bitmap to these "true" observed variables to provide for the statistical parameters (σ, R, P_G and gross error indicator) in the third part

C.1 ASCAT

Decriptor number	Decriptor name	Units
001007	satellite identifier	code table
001012	direction of motion of moving observing	degree tru
002021	satellite instrument data used in process	flag table
004001	year	year
004002	month	month
004003	day	day
004004	hour	hour
004005	minute	minute
004006	second	second
005002	latitude (coarse accuracy)	degree
006002	longitude (coarse accuracy)	degree
002111	radar incidence angle	degree
002112	radar look angle	degree
021192	radar back scatter	db
021193	noise figure	%
021195	missing packet counter	numeric
002111	radar incidence angle	degree
002112	radar look angle	degree
021192	radar back scatter	db
021193	noise figure	%
021195	missing packet counter	numeric
002111	radar incidence angle	degree
002112	radar look angle	degree
021192	radar back scatter	db
021193	noise figure	%
021195	missing packet counter	numeric
011012	wind speed at 10 m	m/s
011011	wind direction at 10 m	degree tru
021197	uwi product confidence	flag table
222000	quality information follow	
031002	extended delayed descriptor replication	numeric
031031	data present indicator	numeric
------	(29 times)-------	-------
001031	generating centre	code table
001201	generating application	code table
031002	extended delayed descriptor replication	numeric
033007	% confidence	numeric
------	(29 times)-------	-------
235000	cancel backward data reference	
001031	generating centre	code table
001201	generating application	code table
031002	extended delayed descriptor replication	numeric
02111	radar incidence angle	degree
002112	radar look angle	degree
021192	radar back scatter	db
021193	noise figure	%
021195	missing packet counter	numeric
002111	radar incidence angle	degree
002112	radar look angle	degree
021192	radar back scatter	db
021193	noise figure	%

Descriptor number	Descriptor name	Units
021195	missing packet counter	numeric
002111	radar incidence angle	degree
002112	radar look angle	db
021192	radar back scatter	%
021193	noise figure	numeric
021195	missing packet counter	numeric
236000	backward reference bit map	numeric
224000	first order statistics follow	
031002	extended delayed descriptor replication	
031031	data present indicator	-------
------	(15 times)-------	code table
001031	generating centre	code table
001201	generating application	code table
008023	first order statistics	numeric
031002	extended delayed descriptor replication	
224255	first order statistics value marker	-------
------	(3 times)-------	

C.2 ATOVS

Descriptor number	Descriptor name	Units
001007	satellite identifier	code table
004001	year	year
004002	month	month
004003	day	day
004004	hour	hour
004005	minute	minute
004006	second	second
005002	latitude (coarse accuracy)	degree
006002	longitude (coarse accuracy)	degree
007022	solar elevation	degree
002025	satellite channel (s) used in computation	flag table
002022	satellite data processing technique used	flag table
027020	satellite location counter	numeric
008003	vertical significance (satellite observation)	code table
015001	ozone	dobson
008003	vertical significance (satellite observation)	code table
010004	pressure	pa
020010	cloud cover (total)	%
008003	vertical significance (satellite observation)	code table
008012	land/sea qualifier	code table
010001	height of land surface	m
012061	skin temperature	k
010004	pressure	pa
008003	vertical significance (satellite observation)	code table
007004	pressure	pa
007004	pressure	pa
012007	virtual temperature	k
------	(15 times the last 3 parameters)-------	-------
008003	vertical significance (satellite observation)	code table
007004	pressure	pa
013016	precipitable water	kg/m**2
------	(3 times the last 3 parameters)-------	-------
008003	vertical significance (satellite observation)	code table
012062	equivalent black body temperature	k
------	(40 times)-------	-------
008003	vertical significance (satellite observation)	code table
010004	pressure	pa
012001	temperature/dry bulb temperature	k
222000	quality information follow	numeric
031002	extended delayed descriptor replication	numeric
031031	data present indicator	
------	(123 times)-------	-------
001031	generating centre	code table
001201	generating application	code table
031002	extended delayed descriptor replication	numeric
033007	% confidence	numeric
------	(123 times)-------	-------
235000	cancel backward data reference	code table
001031	generating centre	code table
001201	generating application	numeric
031002	extended delayed descriptor replication	k

Descriptor number	Descriptor name	Units
012062	equivalent black body temperature	-------
------	(40 times)-------	numeric
224000	first order statistics follow	numeric
236000	backward reference bit map	
031002	extended delayed descriptor replication	-------
031031	data present indicator	code table
------	(40 times)-------	code table
001031	generating centre	code table
001201	generating application	numeric
008023	first order statistics	
031002	extended delayed descriptor replication	-------
224255	first order statistics value marker	
------	(40 times)-------	
224000	first order statistics follow	code table
237000	use previously defined bit map	code table
001031	generating centre	code table
001201	generating application	numeric
008023	first order statistics	
031002	extended delayed descriptor replication	-------
224255	first order statistics value marker	
-------	(40 times)-------	
222000	quality information follow	code table
237000	use previously defined bit map	code table
001031	generating centre	numeric
001201	generating application	numeric
031002	extended delayed descriptor replication	-------
033241	gross error probability	
-------	(40 times)-------	
222000	quality information follow	code table
237000	use previously defined bit map	code table
001031	generating centre	numeric
001201	generating application	code table
031002	extended delayed descriptor replication	-------
033242	gross error indicator	
-------	(40 times)-------	

APPENDIX D : ACRONYMS AND ABBREVIATIONS

AIREP: WMO code for single level upper air reports from aircraft or balloon of wind and temperature
AMSU: Advanced Microwave Sounding Unit
ASCAT: Advanced SCATterometer
ATOVS: Advanced TIROS-N Operational Vertical Sounder
BUFR: Binary Universal Format Representation
BUOY: WMO code for ocean surface reports of meteorological and oceanographic parameters from a buoy
CMA: Central Memory Array
DWL: Doppler Wind Lidar
ECMWF: European Centre for Medium-range Weather Forecasts
ERS: European Remote-sensing Satellite
ESA: European Space Agency
FOV: Field-Of-View
GRIB: GRId in Binary
GTS: Global Telecommunication System
HIRS: High-resolution Infra-red Radiation Sounder
IASI: Infra-red Atmospheric Sounding Interferometer
IFS: Integrated Forecasting System
METOP: METeorological Operational polar Platform
MSU: Microwave Sounding Unit
NESDIS: National Environmental Satellite, Data and Information Service (of NOAA)
NOAA: National Oceanic and Atmospheric Administration (of the USA)
NWP: Numerical Weather Prediction
OI: Optimal Interpolation
OSSE: Observing System Simulation Experiment
PAOB: WMO code for bogus surface pressure observations derived from imagery and ancillary information
PILOT: WMO code for vertical sounding reports of wind only
RTTOV: Software package for fast radiative transfer computations for TOVS channels
SATOB: WMO code used for satellite data, including cloud-tracked winds
SHIP: WMO code for ocean surface reports of meteorological parameters from a moving platform
SST: Sea Surface Temperature
SSU: Stratospheric Sounding Unit
SYNOP: WMO code for surface reports of meteorological parameters
TEMP: WMO code for vertical sounding reports of height, wind, temperature and humidity
TOVS: TIROS-N Operational Vertical Sounder
UT: Universal Time
WMO: World Meteorological Organization

APPENDIX E: EXTERNAL ORGANISATION OF DATABASE AND MEANS OF ACCESS

The database is stored for ESA at ECMWF. The format of the database is BUFR for simulated observations and GRIB for the nature run fields produced by the model. To obtain the database, users have to apply to ESA through the Head of the Earth Sciences Division, ESTEC and, after ESA's acceptation, ECMWF will provide access. ECMWF can provide users with BUFR and GRIB decoding libraries, plus an example of specific software for decoding the OSSE database and the nature run fields, on the basis of a standard agreement on the provision of ECMWF software.

The nature run fields are stored every six hours in sets of binary GRIB files, and can be retrieved using the ECMWF's MARS software (MARS User Guide, ECMWF Meteorological Bulletin M1.9/2, 1993). The nature run fields are identical to the ones of the first project, and are described in Appendix E of the first contract report (*Stoffelen et al*, 1994). The simulated observations are stored in sets of daily binary BUFR files, the files for day D containing all observations between 00:30 UT at day D and 00:30 UT at day D+1. In the ECMWF storage system (ECFILE) the files are kept on the path:

/RDX/ESA/DWL_OSSE/

The different observation types of the first and second projects are grouped in the set of BUFR files:

- file **bufrsynopYYMMDD** for the date **YYMMDD**, containing land SYNOPs, SHIPs, BUOYs, AIREPs, TEMPs, PILOTs, PAOBs and SATOBs (approximate size: 2.5 Mbyte).
- file **bufrtovsYYMMDD**, containing TOVSs (approximate size: 6.5 Mbyte).
- file **bufIdwlJYYMMDD**, containing DWLs for instrument scenario **I** and orbit scenario **J** (approximate size for low resolution scenarios: 18 Mbyte). **J** is 1 for the 800 km orbit and 2 for the 525 km orbit. **I** is 1 for the 10 Joule instrument, 2 for the 5 Joule descoped instrument and 3 for the 10 Joule instrument with 9.5 Hz sampling rate (high resolution data run on 930206).
- file **bufrscattYYMMDD**, containing ASCAT backscatter measurements (approximate size 5 Mbyte).
- file **bufratovsYYMMDD**, containing ATOVs (approximate size: 9 Mbyte).

Each file consists of a set of BUFR messages. As BUFR is a table driven format, three BUFR binary tables are needed to decode the files. These tables are the BUFR tables currently used at ECMWF:

- table B: **B000980201** (classification of elements)
- table C: **C000980201** (text and meaning of code and flag tables)
- table D: **D000980201** (list of common sequences)

A full definition of the BUFR format can be found in the WMO publication No. 306 (Manual on Codes Volume I, Part B).